Mon. Not. R. astr. Soc. (1978) **182**, 797–799

The structure of the isophotes of elliptical galaxies

David Carter★ *Institute of Astronomy, Madingley Road, Cambridge*

Received 1977 August 3; in original form 1977 February 10

Extended summary. Models of elliptical galaxies, such as those of Prendergast & Tomer (1970); Wilson (1975); Gott (1975) and Larson (1975) make predictions of the shapes of the isophotes of elliptical galaxies. This paper describes procedures for measurement of parameters representing the shapes of the isophotes of elliptical galaxies, and presents results for a sample of 19 elliptical and S0 galaxies in the region of the clusters Abell 2197 and Abell 2199.

The main data reduction was done from a IIIaJ plate of this region of the sky taken with the Palomar 48-in. Schmidt. The plate was scanned with the Herstmonceux PDS 1010A microdensitometer, a raster some 4–9 mm square at 15 μm resolution (1 arcsec) around each galaxy being scanned. The effects of the brightest field stars and other galaxies were removed from the scans as described previously (Carter 1977a). Selected isophotes of the galaxies were then extracted from the raster scans as a series of (x, y) coordinates, and to each the best-fit ellipse was determined. This is defined by five parameters, the centre (x_0, y_0), the major and minor axes and θ, the orientation of the major axis.

The isophote is then transformed to rectified coordinates, in which a perfect ellipse would be circular. The rectified isophote is then examined for deviations from circularity by Fourier analysis of the radius of the circle $R_i = (x_i^2 + y_i^2)^{1/2}$ as a function of $\phi_i = \tan^{-1}(y_i/x_i)$. The first five Fourier components indicate errors in the ellipse-fitting procedure, and indeed, such a systematic error was found, interpreted and corrected for. The third and fourth-order components indicate systematic deviations from ellipticity, that most likely to be systematically non-zero is the fourth-order cosine component, B_4. B_4 is zero for a perfect ellipse, negative for an isophote which is somewhat 'box-shaped' (Prendergast & Tomer 1970), and positive for an isophote. ϵ was corrected for the effects of smoothing due to seeing, which

The major and minor axes of the fitted ellipse were were transformed to $R = (ab)^{1/2}$ and $\epsilon = 10(a-b)/a$, the average radius and ellipticity of each isophote. ϵ was corrected for the effect of something due to seeing, which was assumed to be Gaussian smoothing, and for the real Gaussian smoothing

★ Present address: Department of Astrophysics, South Parks Road, Oxford.

which was applied for faint isophotes to reduce noise. The correction was determined by experimental Gaussian smoothing on an image obeying a Hubble-like surface brightness law.

Ellipticity, position angle and B_4 are plotted against radius for 15 of the galaxies whose images are not too circular. Where residual star images or the haloes of nearby galaxies distort the isophotes noticeably these isophotes are not used. No measurement at radii below 10 arcsec is used as the observed isophote shape is dominated by the point-spread function. Errors in the fitting procedure are small, and the errors adopted are defined by the local scatter of the points, due to unremoved faint images. The results can be summarized as follows:

(1) ϵ generally increases with radius and then tends to a constant, it increases by amounts of order one. This is especially true for the brightest galaxies, the cD galaxies NGC 6166 and 6173 and NGC 6146 and 6160 which are bright elliptical galaxies. Exceptions to this include some fainter galaxies, where the results are less dependable, and NGC 6159, some distance from the clusters, where ϵ is constant.

(2) B_4 does not depart systematically from zero by more than a few per cent. In some galaxies, such as NGC 6166 it tends to be negative, but in others such as NGC 6146 and galaxy 13 (III Zw 82) it tends to be positive.

(3) θ varies with radius by up to 0.3 rad (18°). This is most noticeable in NGC 6173 and 6146, but also occurs in some fainter galaxies. Projection effects mean that the rotation of ellipsoids of constant density could be greater.

Systematic errors originate from three sources, the plate, the microdensitometer and the sky. Effects due to the plate and the microdensitometer occur at high densities and high density gradients, the highest encountered here are a density of 2.0 D and a gradient of 0.3 D/resolution element. Studies of photographic effects and experience with this microdensitometer indicate that such effects here should be small.

Data from a deep 127-04 plate for five brighter galaxies were similarly analysed, and agree well with the previous data. Differences are due to two factors, saturation of the 127-04 plate and the larger point spread function at red wavelengths. Thus it seems that photographic effects do not cause serious errors. Errors due to superfluous images were analysed by a detailed study of the isophotes and fits for NGC 6166. Such distortions will cause scatter but not systematic errors in the parameters. A closeness of fit parameter was derived from each isophote and tabulated, the fit becomes gradually worse as the radius increases.

The trend for ellipticity to increase with radius agrees with the results of several previous authors, who have investigated Virgo ellipticals (Liller 1960, 1966; Arp & Bertola 1969; King, private communication) and dwarf ellipticals (Hodge 1963, 1973, 1976). King has also found significant variations of position angle with radius in Virgo cluster ellipticals.

The models of Prendergast & Tomer (1970) and Wilson (1975) involve steady-state solutions of the non-linear Poisson equation. Both of these predict an ellipticity profile somewhat peaked, in conflict with observation.

Larson (1975) considers the collapse of a gas cloud, with star formation taking place during the collapse. The models with high turbulent viscosity show a less peaked ellipticity distribution, resembling the observations more closely. Gott (1975) considers the collapse of a cloud of stars, and predicts ellipticity decreasing with radius, which does not agree with the observations. Lynden-Bell (1967) showed in an asymptotic approximation that the ellipticity of the isophotes should tend to a constant at large radii, but the theory of violent relaxation of rotating systems is not sufficiently rigorous to determine the distribution function.

Binney (1976), considering violent relaxation after anisotropic collapse, showed that this led to a flattened equilibrium system, but his calculations were not sufficiently detailed to predict the ellipticity distribution with radius.

The variation of position angle with radius appears to be a real effect. There are two plausible explanations, either the outer regions of the galaxy are not relaxed, due to accretion or tidal disturbance, or the galaxy could be in a triaxial equilibrium state (*cf.* Stark 1977).

A further asymmetry is indicated by the observations, it appears that the centres of the outer isophotes of NGC 6166 and 6173 are somewhat displaced from the nuclei. This again appears to be a real effect, and its cause is not clear.

The full text of this paper appears on *Microfiche* MN 182/2.

Monthly Notices
of the
ROYAL ASTRONOMICAL SOCIETY

VOL. 182, NO. 3, 1978

The structure of the isophotes of elliptical galaxies

David Carter

Published for the Royal Astronomical Society

Blackwell Scientific Publications

Oxford Microform Publications

The microfiches are 105 x 148mm archivally permanent silver halide film produced to internationally accepted standards in the NMA 98-image format

Microfiches produced by O.M.P., Blue Boar St., Oxford OX1 4EY and Micromedia, Bicester, Oxon

C01

SUMMARY

From data obtained by scanning Palomar Schmidt plates, taken with IIIaJ and 127-04 emulsions, with a fast two-dimensional micro-densitometer, parameters representing the structure of the isophotes of elliptical galaxies are determined. Ellipticity, position angle of the major axis, and low order Fourier components are determined as a function of radius. The results of this investigation are presented in tabular and graphical form, and it is seen that in general ellipticity is an increasing or peaked function of radius, and that the higher order moments are small. The implications for various theories of the formation and structure of elliptical galaxies are discussed.

C02

THE STRUCTURE OF THE ISOPHOTES OF ELLIPTICAL GALAXIES

1. Introduction

A number of authors (Prendergast and Tomer 1970, Wilson 1975, Gott 1975, Larson 1975) have constructed models of elliptical galaxies based on stellar dynamics or a combination of stellar dynamics and gas dynamics. These models make predictions of the shapes of the isophotes of the galaxies, and this paper describes measurements of parameters representing the shapes of the isophotes of 19 galaxies in the region of the galaxy clusters Abell 2197 and Abell 2199. The galaxies are listed in Table 1 and are marked on Plate 1, which is an enlargement of this region of the sky on the Palomar sky survey E plate. The values of the parameters measured for these galaxies are compared with the predictions of the models.

2. Data reduction techniques

The plate material used in this investigation consists of a nitrogen baked IIIaJ emulsion plate of this region of the sky taken by C.D. Mackay and R.J.E. Kraft with the Mount Palomar 48 inch Schmidt telescope in 1973. The plate is described in more detail in a previous paper (Carter 1977a). The plate was scanned with the PDS microdensitometer at the Royal Greenwich Observatory. The effects of the brightest field stars were removed from the two dimensional scans as described in Carter (1977a). Selected isophotes of the galaxies were written onto magnetic disc as a set of (x,y) co-ordinates. To each set of (x,y) co-ordinates the best fit ellipse was determined by minimising the quantity:

$$S = \sum_i \left\{ \frac{[(x_i - x_0)\cos\theta + (y_i - y_0)\sin\theta]^2}{a^2} + \frac{[y_i - y_0)\cos\theta - (x_i - x_0)\sin\theta]^2}{b^2} - 1 \right\}^2 \quad (1)$$

with respect to a, b, x_0, y_0, and θ, thus determining the major axis, minor axis, centre (x_0, y_0) and position angle of the major axis of the best fit ellipse.

C03

TABLE 1

GALAXY	NGC	ZWICKY[1]	ZWICKY AND HERZOG[2]	ROOD AND SASTRY[3]	MAGNITUDE[4]	TYPE[5]
1	6166		16 26.9 + 39 40	85	13.9	cD4
2	6173		16 28.1 + 40 55		14.0	cD4
3	6146		16 23.5 + 41 01		13.8	E3
4	6160		16 26.0 + 41 02		14.8	DE3
5	6159		16 25.8 + 42 47		15.2	DE3
6	6180		16 28.9 + 40 40		15.2	E3
7	6158		16 26.0 + 39 30	52	15.5	E3
8			16 26.2 + 39 22	61	15.4	E3
9			16 25.4 + 39 38	38	15.3	E2
10				72	15.5	E1
11				62	16.0	E2
12			16 26.0 + 42 45		15.5	E2
13		III Zw 82	16 27.7 + 40 59		15.5	E1
14				76	15.5	E1
15		III Zw 79			16.0	E1
16			16 29.6 + 39 16	162	15.5	E0
17			16 29.4 + 39 54	159	14.8	S0
18			16 24.7 + 41 01		15.7	E0
19				64	16.5	E0

1 Catalog of selected compact and post eruptive galaxies.

2 Catalog of galaxies and clusters of galaxies, Vol. III.

3 Rood and Sastry (1972).

4 From Zwicky and Herzog, or estimated from the plate.

5 Estimated from the plate.

C05 C06

The isophote is then transformed to rectified co-ordinates by the following transformations:

$$x_i' = \frac{(x_i - x_0)\cos\theta + (y_i - y_0)\sin\theta}{a} ,$$

$$y_i' = \frac{(y_i - y_0)\cos\theta - (x_i - x_0)\sin\theta}{b} .$$

The isophote in rectified co-ordinates is then examined for deviations from circularity, which represent deviations of the original isophote from the ellipse found by the fitting procedure. This is done by Fourier analysis of the quantity $R_i = (x_i^2 + y_i^2)^{\frac{1}{2}}$ as a function of $\phi_i = \tan^{-1}(y_i/x_i)$.
The Fourier components are given by

$$A_0 = \frac{1}{2\pi}\int R(\phi)\, d\phi ,$$

$$A_n = \frac{1}{\pi}\int R(\phi)\sin n\phi\, d\phi \qquad n = 1,2,\ldots ,$$

$$B_n = \frac{1}{\pi}\int R(\phi)\cos n\phi\, d\phi \qquad n = 1,2,\ldots .$$

The first five Fourier components, $(A_0 - 1)$, A_1, B_1, A_2, and B_2 indicate errors in the fitting procedure, if any of these quantities approach 0.1 then the fit is in error, and the isophote is not used in the analysis.

In practice A_0 is always slightly less than 1 for a noisy isophote. The reason for this is that the fitting procedure minimises the quantity $\sum_i [R_i^2 - 1]^2$, and not $\sum_i [R_i - 1]^2$. Because of this positive deviations in R_i have more effect on the fit than negative deviations, and the fit gives a radius systematically too large. This is corrected for by multiplying a and b by A_0, and dividing all of the other

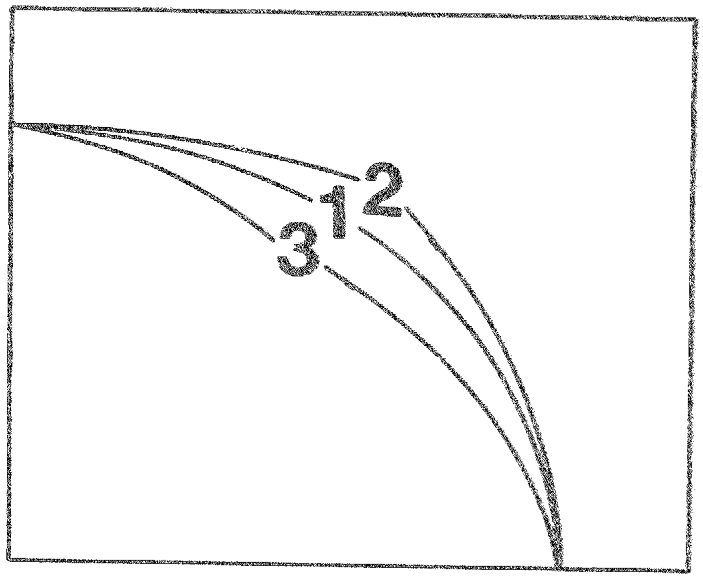

Figure 1 - Isophote shapes. Curve 1 is an ellipse, with $B_4 = 0$, curve 2 has negative B_4 and curve 3 positive B_4. Only a quarter of each isophote is shown.

Fourier components by A_0. Of the other Fourier components the one which is most likely to be systematically non-zero is B_4. Figure 1 shows the types of isophotes which would give certain values of B_4. Curve 1 is a perfect ellipse which would give $B_4 = 0$, curve 2 is a somewhat rectangular isophote which would give negative B_4, curve 3 is of the type predicted by Larson (1975) for some of his models, and would give positive B_4.

The same information can be extracted from the scans in two other slightly different ways.

(1) The centre of the image (x_0, y_0) can be fixed at the light maximum, and the fitting procedure restricted to three free parameters, a, b, and θ. The Fourier analysis is then carried out as before, and the Fourier components A_1 and B_1 represent the deviation of the actual centre of the isophote from the assumed centre.

(2) The centre of the image, average ellipicity and average position angle can be determined for the whole image initially, and then a series of ellipses with these parameters and a variety of average radii are superimposed on the image. The procedure is then to follow the ellipse around the image, taking measurements of the light intensity at intervals. This intensity is then Fourier analysed as a function of ϕ and this Fourier analysis gives the parameters required. This technique is discussed by Kibblewhite (1969).

Each of the two above methods is equivalent in principle to the method used.

The procedure used suffers from two main weaknesses.

(1) The fitting procedure minimises $\sum_i [R_i^2 - 1]^2$ rather than $\sum_i [R_i - 1]^2$. This makes the fit more sensitive to noise than it would otherwise be.

(2) The star removal program replaces a star with a constant density value (Carter 1977a). Isophotes thus remain distorted by the residual star image.

For these two reasons method 2 outlined above would be objectively preferable from the point of view of minimising errors. The procedure for this method would however be much more difficult to implement, and would require much more computer time to run.

A slightly simpler method of reducing the effect of foreground stars on the isophotes would be to plot the deviations of each point on the isophote from the best fit ellipse against ϕ, and then to reject any point which deviated by more than say 3σ from this ellipse. The procedure would then be repeated until no points were rejected. This would reduce noise due to foreground stars, but the risk would be run of rejecting real deviations from ellipticity.

The parameters from the fit are transformed to $R = (ab)^{\frac{1}{2}}$ and $\varepsilon = 10(a-b)/a$, the average radius and ellipticity of each isophote. A correction is applied to ε for the effect of smoothing due to seeing. Experiments on numerical Gaussian smoothing of artificial galaxy images show that such smoothing causes isophotes to appear systematically rounder than they really are, the effect being greatest for isophotes of small average radius. The amount by which the ellipticity is in error because of this effect depends upon ε and (σ/R), where σ is the standard deviation of the Gaussian smoothing profile, and R is the average radius of the isophote. The correction was tabulated as a function of ε and σ/R for an artificial galaxy image who surface brightness distribution is represented by a law similar to Hubble's law:

$$B = B_0 \left(\frac{x^2}{a^2} + \frac{y^2}{b^2} + \alpha^2 \right)^{-1} ,$$

where a and b are of order 1 and α is of order 1 arcsec. This technique for removing the effects of seeing is similar to that used by Hoffman and Crane (1977) for estimating corrections to isophotal galaxy magnitudes.

A star image profile from this plate was determined, and a two component form derived for the profile

$$B = B_0 \exp\left\{\frac{-r^2}{2\sigma^2}\right\} \qquad 0 \leq r \leq 5 \text{ arcsec} ,$$

$$B = B_0 r^{-\alpha} \qquad 5 < r \leq 30 \text{ arcsec} ,$$

where $\sigma = 1.9$ arcsec and $\alpha = 3{\cdot}8$ for this plate. As the fall off in the light level beyond 5 arcsec is rapid only a small percentage of the light is contained in this part of the profile. A Gaussian with standard deviation 1.9 arcsec is therefore a good representation of the seeing profile, and it is on this basis that to correction to ε is made.

Where the image is numerically smoothed to reduce noise in the outermost isophotes the error caused in ε is corrected for in the same way.

3. Results

Figures 2 to 16 are plots of ε, θ, and B_4 against average radius for fifteen of the galaxies in Table 1. Complete sets of data are presented in tabular form in Appendix A for four of the galaxies, galaxies 1, 2, 5 and 11. Complete sets of data for all nineteen galaxies exist and are available on request. Where star images distort the isophotes noticeably the contours are not used, hence there are gaps in the data at some points.

No measurements at radii less than 10 arcsec are used, as here the point spread function dominates the observed isophote shape.

The errors in ε, θ and B_4 due to the fitting procedure are small, and in most cases are within the dimensions of the points in the diagrams. A more realistic error is determined by the scatter of the points in Figures 2 to 16, due to plate noise and unremoved faint stars and residues of images of bright stars. The scatter is estimated from Figures 2 to 16 to be:

$$\delta\varepsilon = 0.2 \quad (r/10 \text{ arcsec})^{\frac{1}{2}},$$

$$\delta B_4 = 0.01 \quad (r/10 \text{ arcsec})^{\frac{1}{2}},$$

$$\delta\theta = 0.1 \quad (r/10 \text{ arcsec})^{\frac{1}{2}} \varepsilon^{-1}.$$

These are the errors on which the error bars in the graphs are based.

The forms of the graphs in Figures 2 to 16 are discussed below.

Galaxy 1 : NGC 6166

This galaxy has a multiple nucleus, which causes the initial decrease in ε and variation in θ. ε increases from a radius of about 30 arcsec and then flattens off. B_4 tends to be negative but very small.

Galaxy 2 : NGC 6173

ε increases from 50 arcsec, and flattens off at a value of about 5. It may decrease again from about 120 arcsec, but here the distortion caused by bright stars imperfectly removed, and also by galaxy 13, causes errors in the parameters. θ varies steadily in the outer regions, the isophotes are slewed round in an anticlockwise sense with increasing radius as seen in Plate 1, the scan being reflected about an axis. B_4 is nowhere significantly different from zero.

Galaxy 3 : NGC 6146

ε increases from just under 3 to about 4 at 50 arcsec, and then flattens off. θ varies steadily at large radii in a clockwise sense with increasing radius. B_4 tends to be positive at large radii.

Galaxy 4 : NGC 6160

ε tends to increase with radius. θ seems fairly constant. B_4 tends to be negative. Due to foreground stars there are gaps and noise in these data.

Galaxy 5 : NGC 6159

NGC 6159 dominates a small group of galaxies some 2 degrees north of Abell 2197, which includes also galaxy 12. Apart from the last two points, which are probably in error due to the proximity of galaxy 12 and a bright foreground star, ε seems constant. θ varies steadily in a clockwise sense with increasing radius. B_4 tends to be negative.

Galaxy 6 : NGC 6180

ε increases slightly at around 30 arcsec. θ shows no systematic trend. B_4 has a tendency to be positive at large radii. This galaxy is described as compact by Zwicky and Herzog (1966).

Galaxy 7 : NGC 6158

This galaxy is also described as compact by Zwicky and Herzog. Nearby faint galaxies contaminate the light distribution and distort the isophotes at large radii, causing gaps and noise in the data. ε is decreasing with radius, but this may be due to contamination. θ is too noisy to draw any conclusions. B_4 is small at all radii.

Galaxy 8

Galaxy 8 is described by Zwicky and Herzog as a double galaxy, the fainter companion distorts the isophotes at large radii. ε appears to decrease with radius, although this result must be treated with scepticism due to the contamination by the fainter companion galaxy. θ is constant and B_4 does not depart significantly from zero.

Galaxy 9

Galaxy 9 is described by Zwicky and Herzog as compact. ε increases somewhat at around 20 arcsec. θ varies steadily in a clockwise sense with increasing radius. B_4 does not deviate significantly from zero.

Galaxy 10

Galaxy 10 is nearly round in the centre, but ε increases to about 1.5 at 25 arcsec. As ε is low θ is very noisy, and no variation is apparent. B_4 is negative at around 20 arcsec, and becomes positive at 35 arcsec.

Galaxy 11

ε is decreasing from a radius of 15 arcsec. θ varies rapidly in an anticlockwise sense with increasing radius. B_4 is small everywhere.

Galaxy 12

Galaxy 12 is a member of the small group of galaxies around NGC 6159. Because of the proximity of NGC 6159 the faintest isophotes are contaminated, and so measurements can only be made out to a radius of some 30 arcsec. ε decreases with radius, θ is constant apart from the last point, which is rotated in an anticlockwise sense, although this is probably not significant. B_4 is small everywhere.

Galaxy 13 : III Zw 82

This galaxy is a very compact elliptical. As it is very close to NGC 6173 the outermost isophotes are contaminated and are not used. ε shows a peak at 20 arcsec, but this may not be significant. θ varies slowly in an anticlockwise sense with increasing radius, although one point differs widely from the others. B_4 tends to be positive.

Galaxy 14

This galaxy is very close to NGC 6166, and the outermost isophotes are contaminated by this galaxy and are not plotted. ε increases, θ is approximately constant but rather noisy and B_4 is small everywhere.

Galaxy 15 : III Zw 79

ε decreases and then increases again at around 20 arcsec. θ varies but not systematically and B_4 is small.

Galaxies 16 to 19 are all nearly round, and although the data are available no conclusions can be drawn.

The results obtained can be summed up by three statements.

(1) ε generally increases with radius and then flattens off. The amount by which it varies is around 1. This is especially true for the brightest galaxies. There are some exceptions to this rule, mostly smaller galaxies in which the region of increase of ε may be too far in to be observed.

(2) B_4 does not depart systematically from zero by more than a few percent. It is not systematically positive or negative.

(3) θ can vary with radius by up to 0.3 radians (18 degrees). Projection effects could mean that the real rotation of ellipsoids of constant density could be even greater.

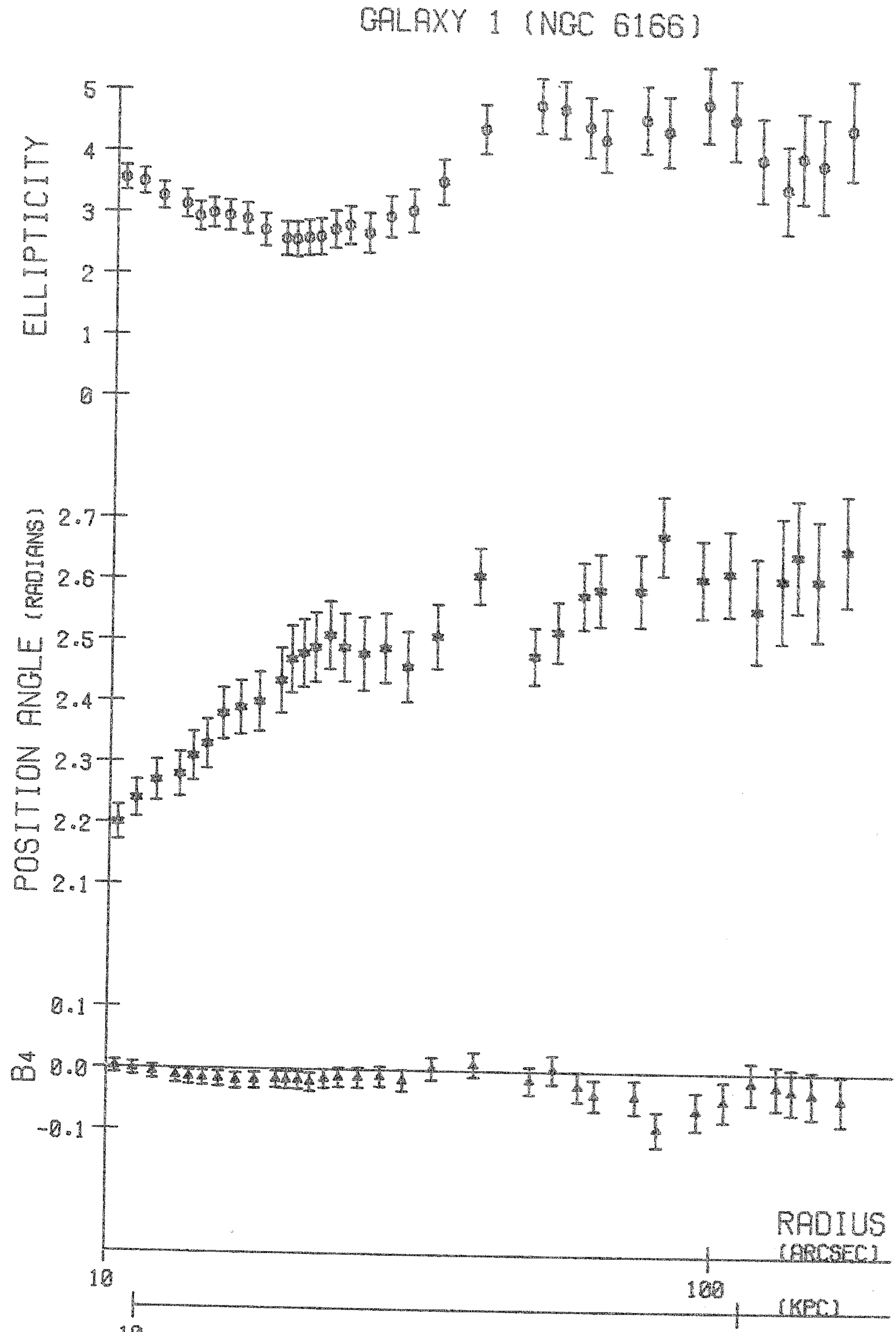

D01 Figure 2 - ε, θ, and B_4 against radius for galaxy 1.

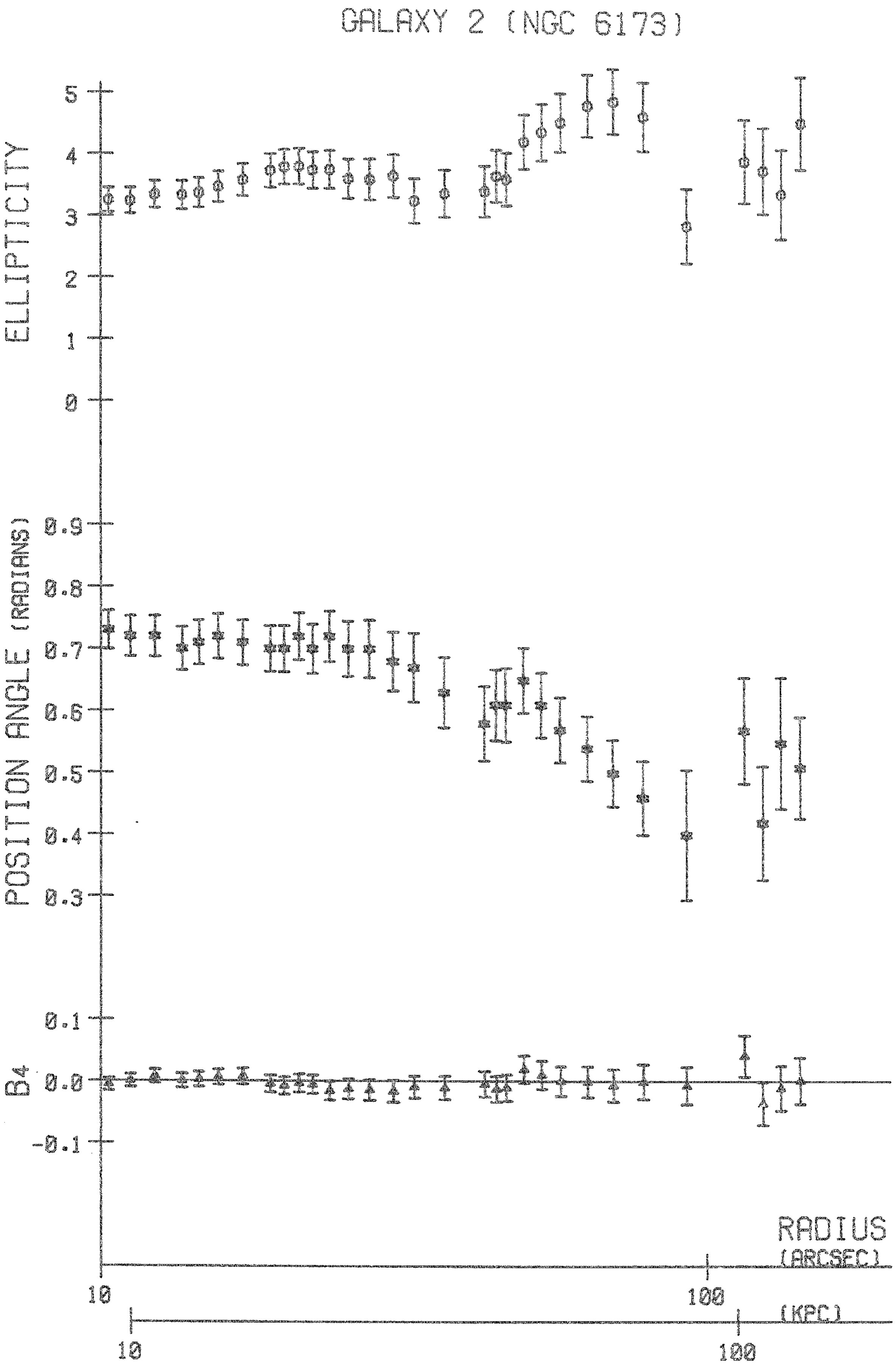

D02 Figure 3 - ϵ, θ, and B_4 against radius for galaxy 2.

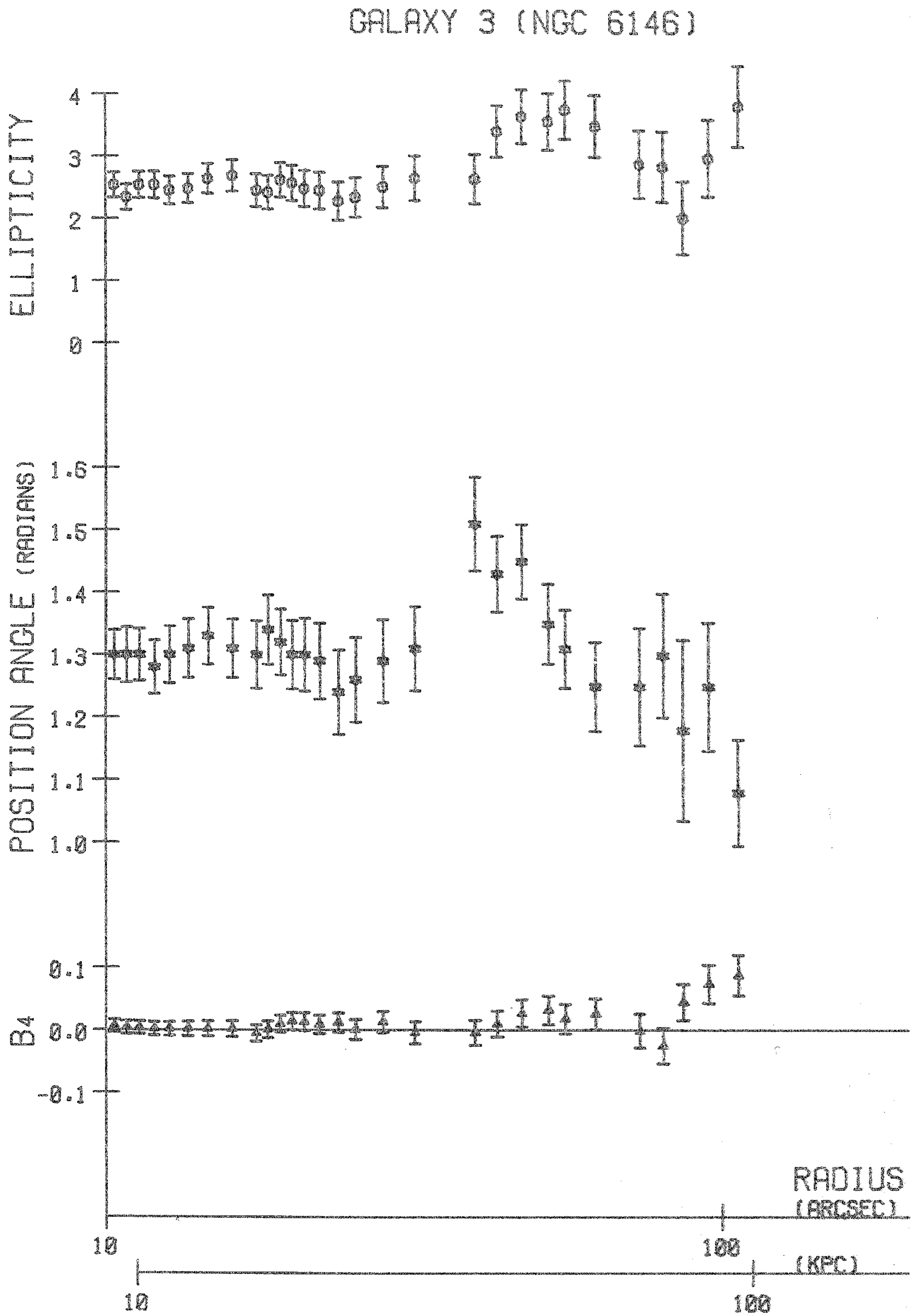

D03 Figure 4 - ε, θ, and B_4 against radius for galaxy 3.

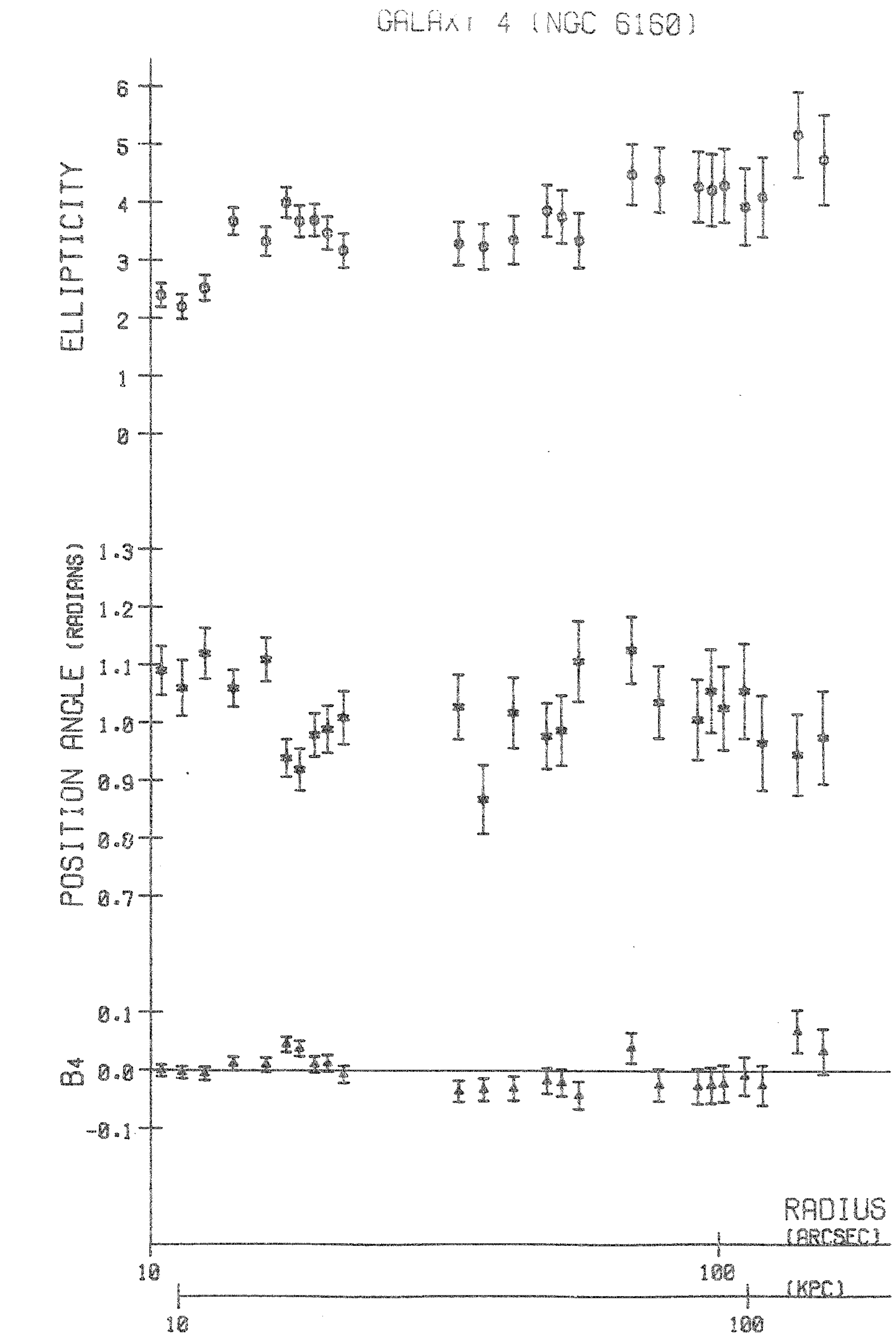

D04 Figure 5 - ε, θ, and B_4 against radius for galaxy 4.

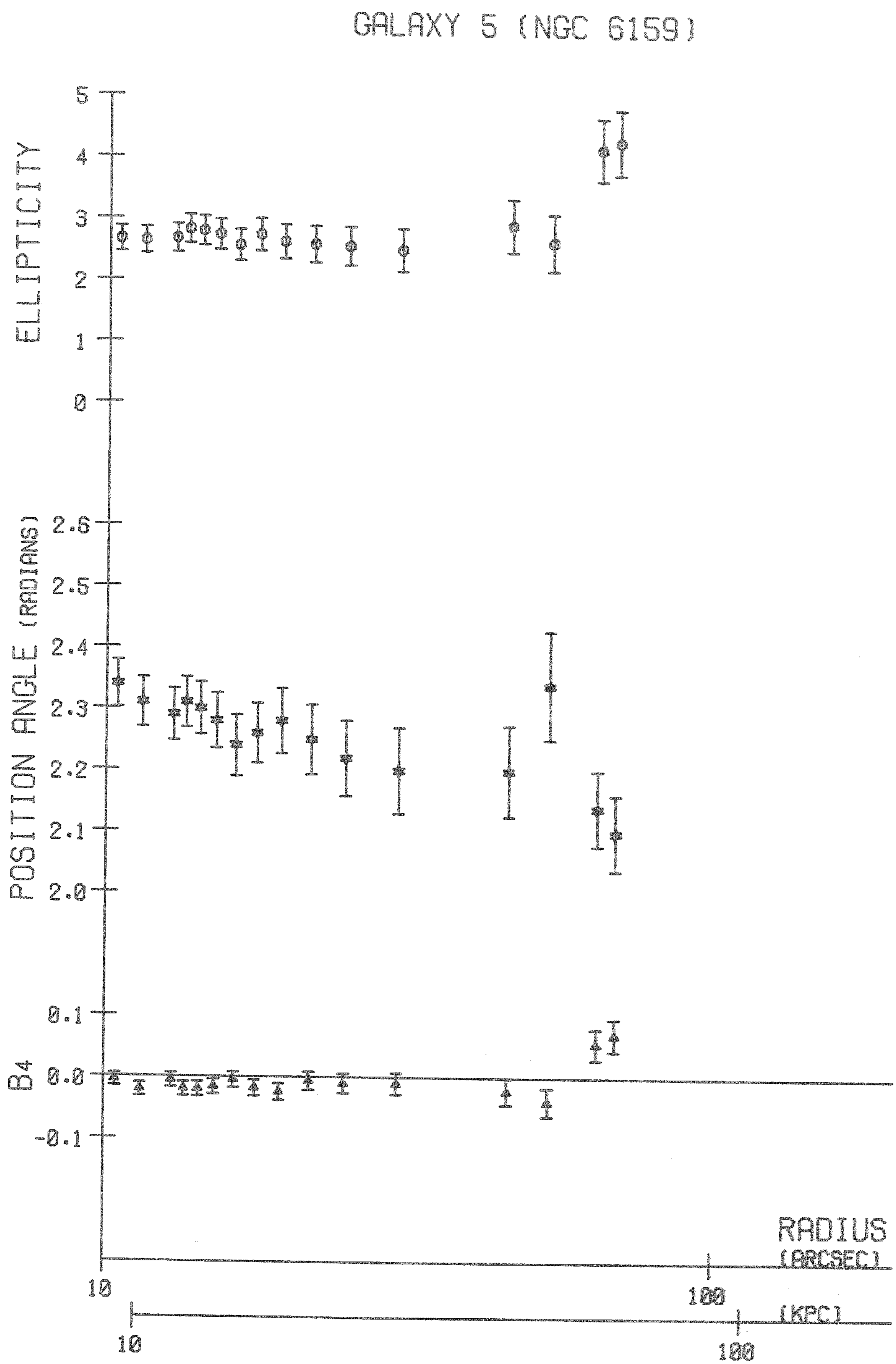

D05 Figure 6 - ε, θ, and B_4 against radius for galaxy 5.

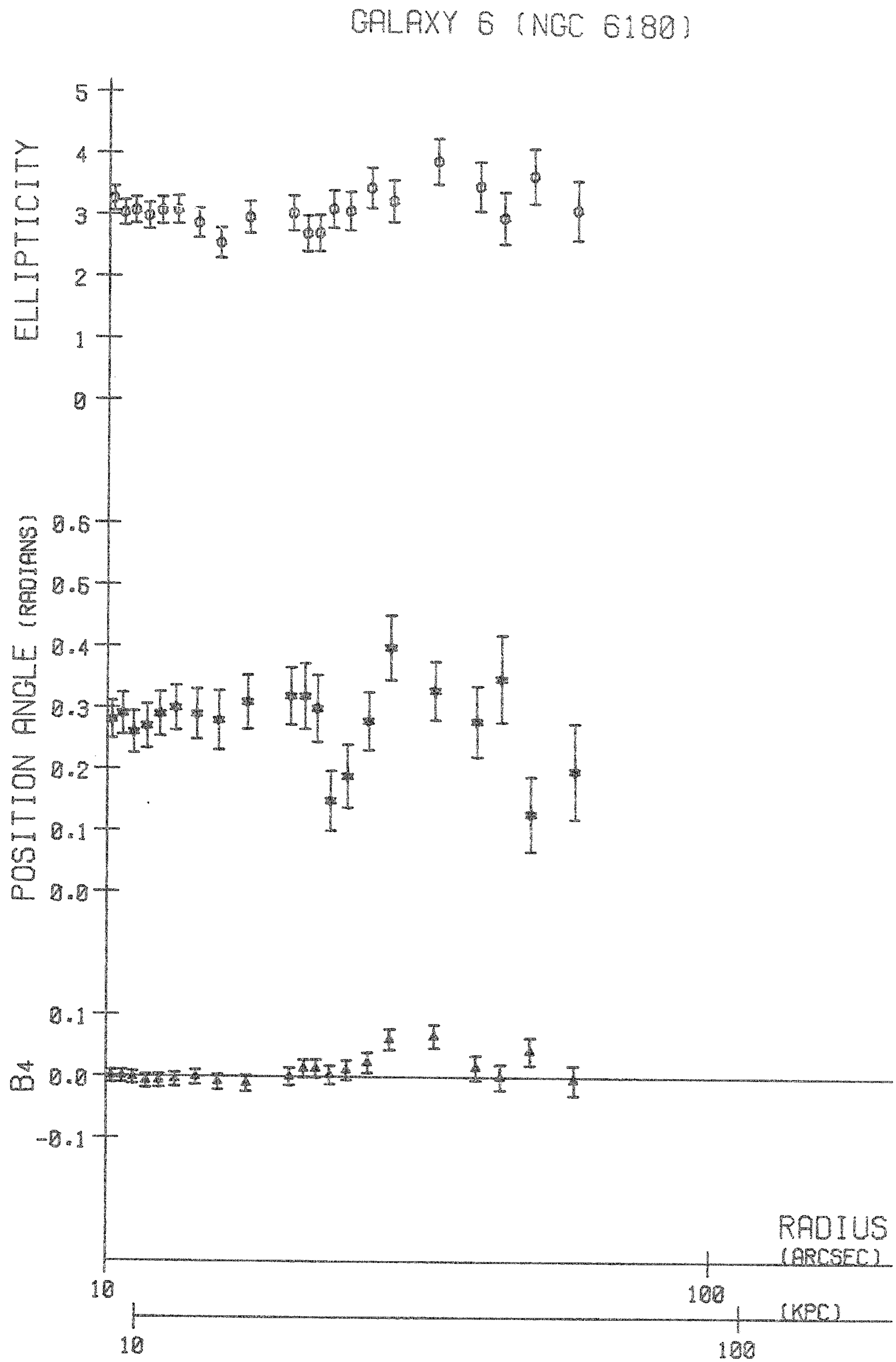

D06 Figure 7 - ε, θ, and B_4 against radius for galaxy 6.

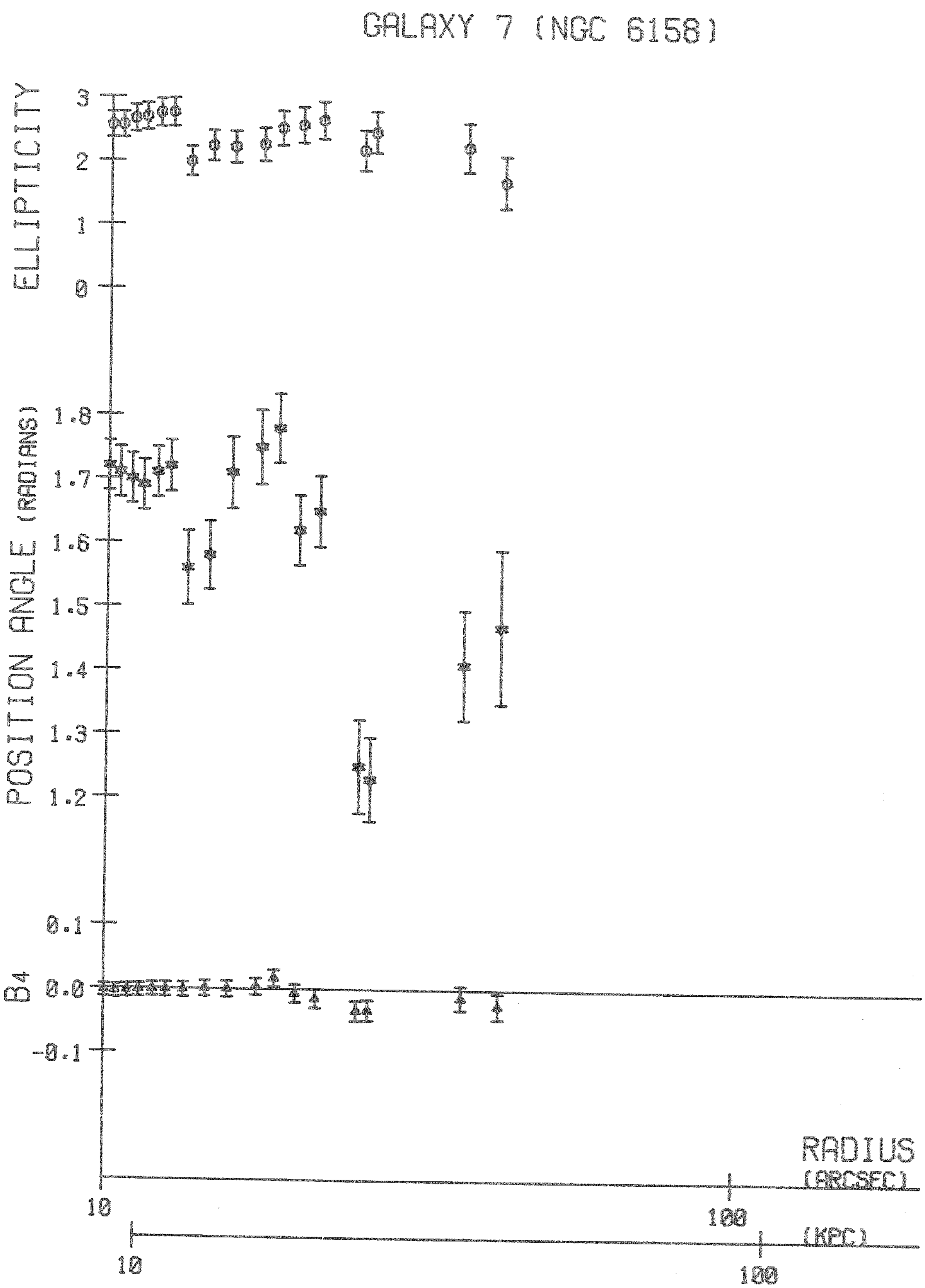

D07 Figure 8 - ϵ, θ, and B_4 against radius for galaxy 7.

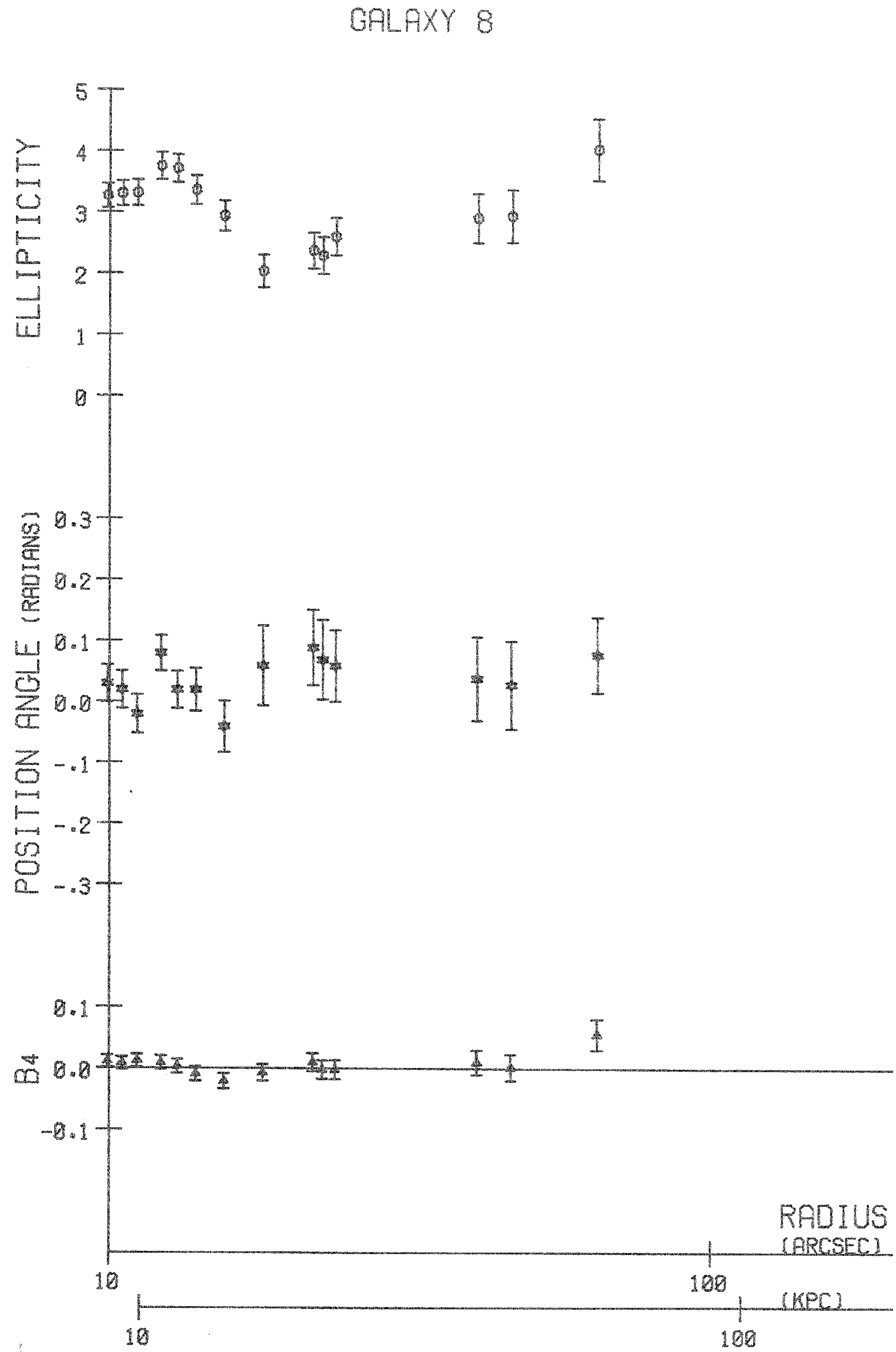

D08 Figure 9 - ε, θ, and B_4 against radius for galaxy 8.

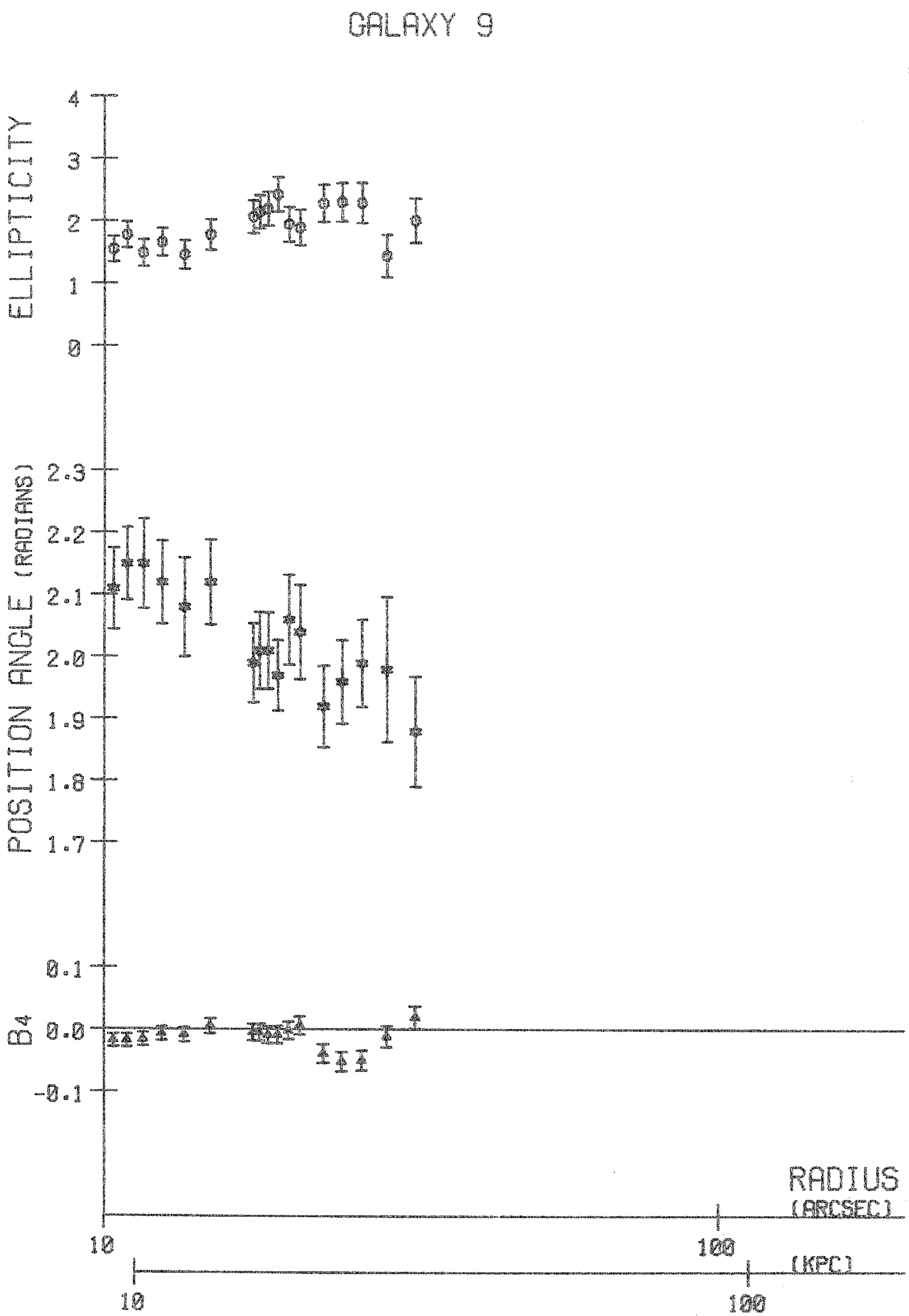

D09 Figure 10 – ε, θ, and B_4 against radius for galaxy 9.

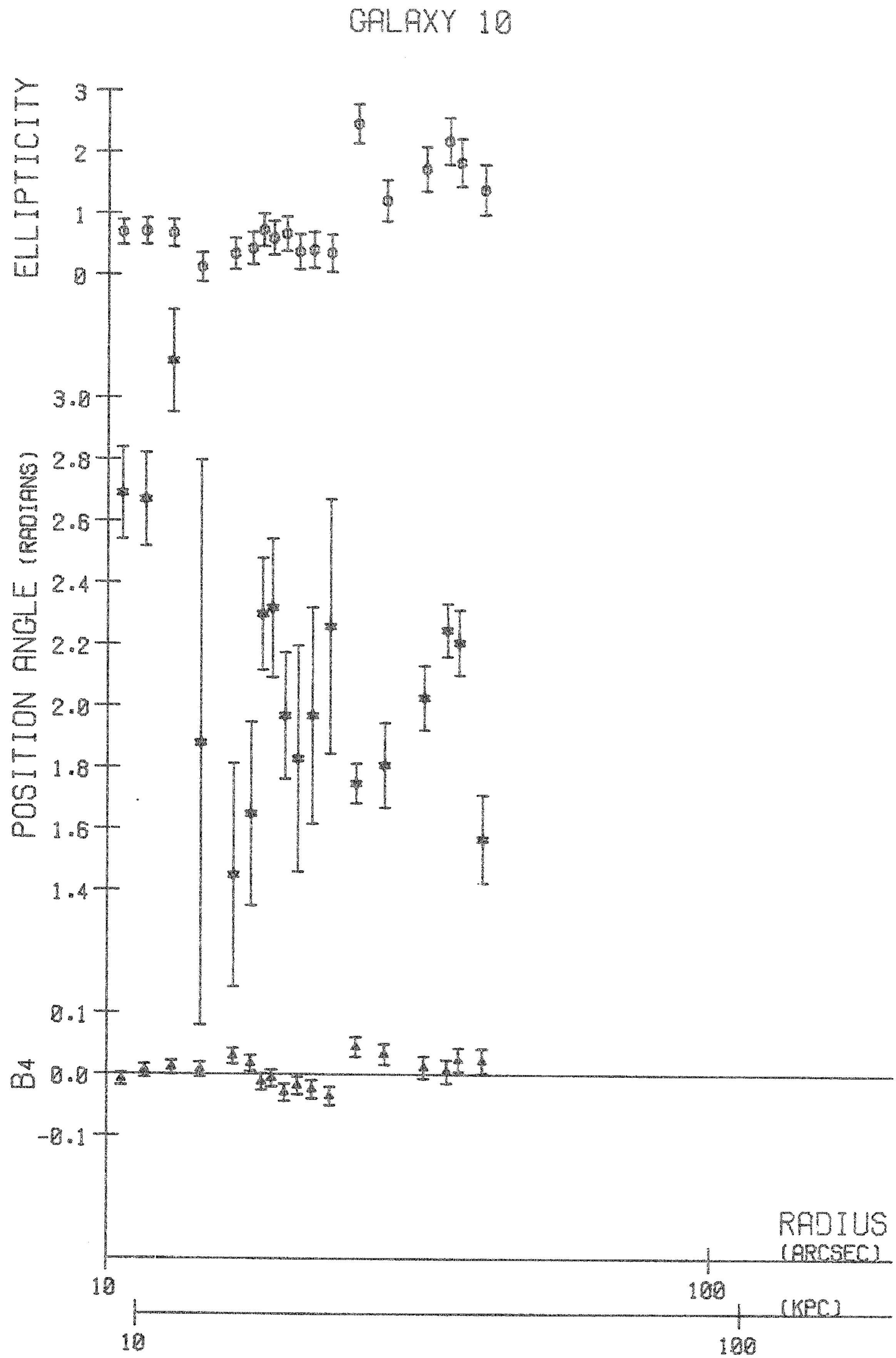

D10 Figure 11 - ε, θ, and B_4 against radius for galaxy 10.

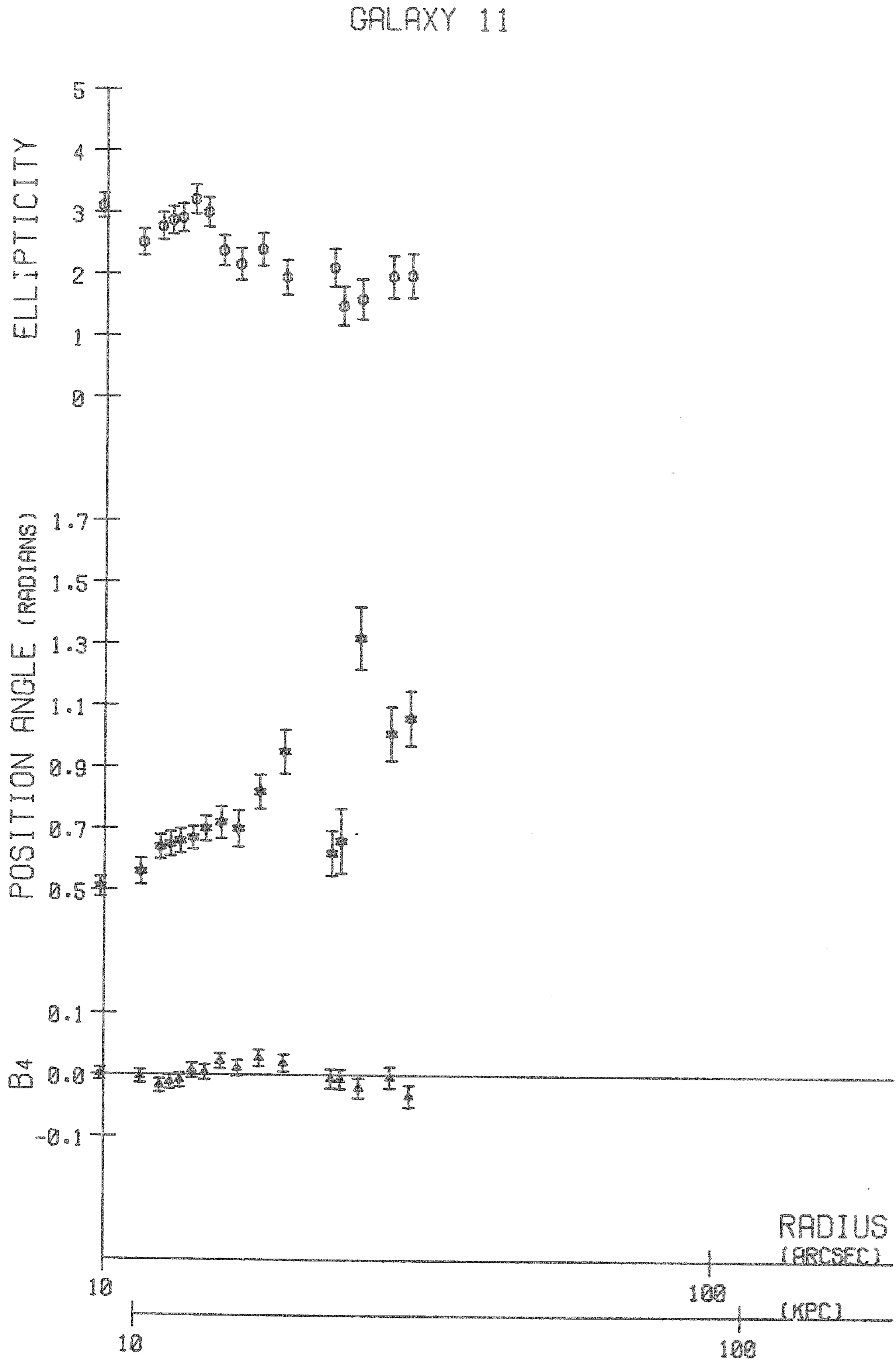

D11 Figure 12 - ε, θ, and B_4 against radius for galaxy 11.

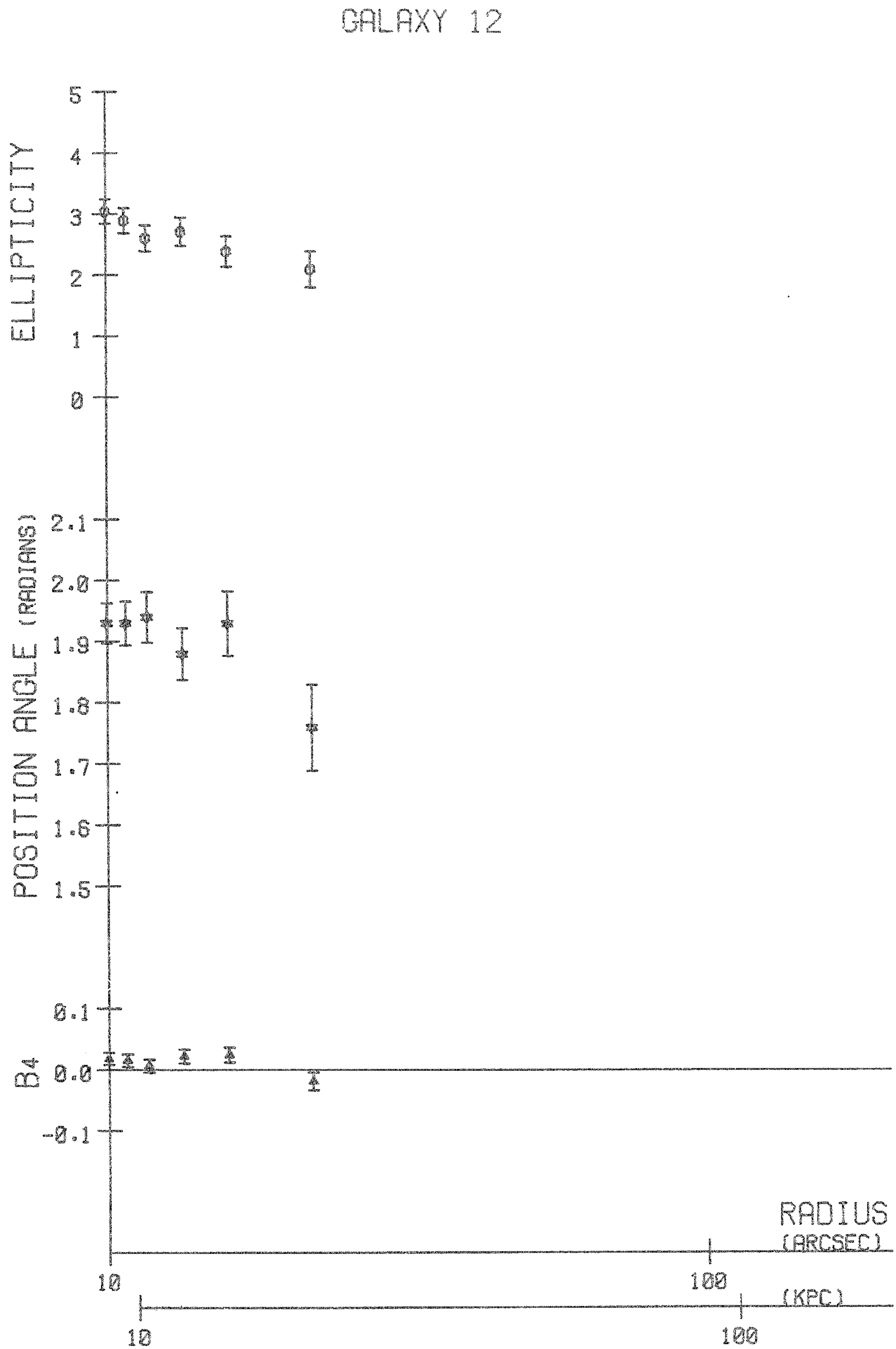

D12 Figure 13 - ε, θ, and B_4 against radius for galaxy 12.

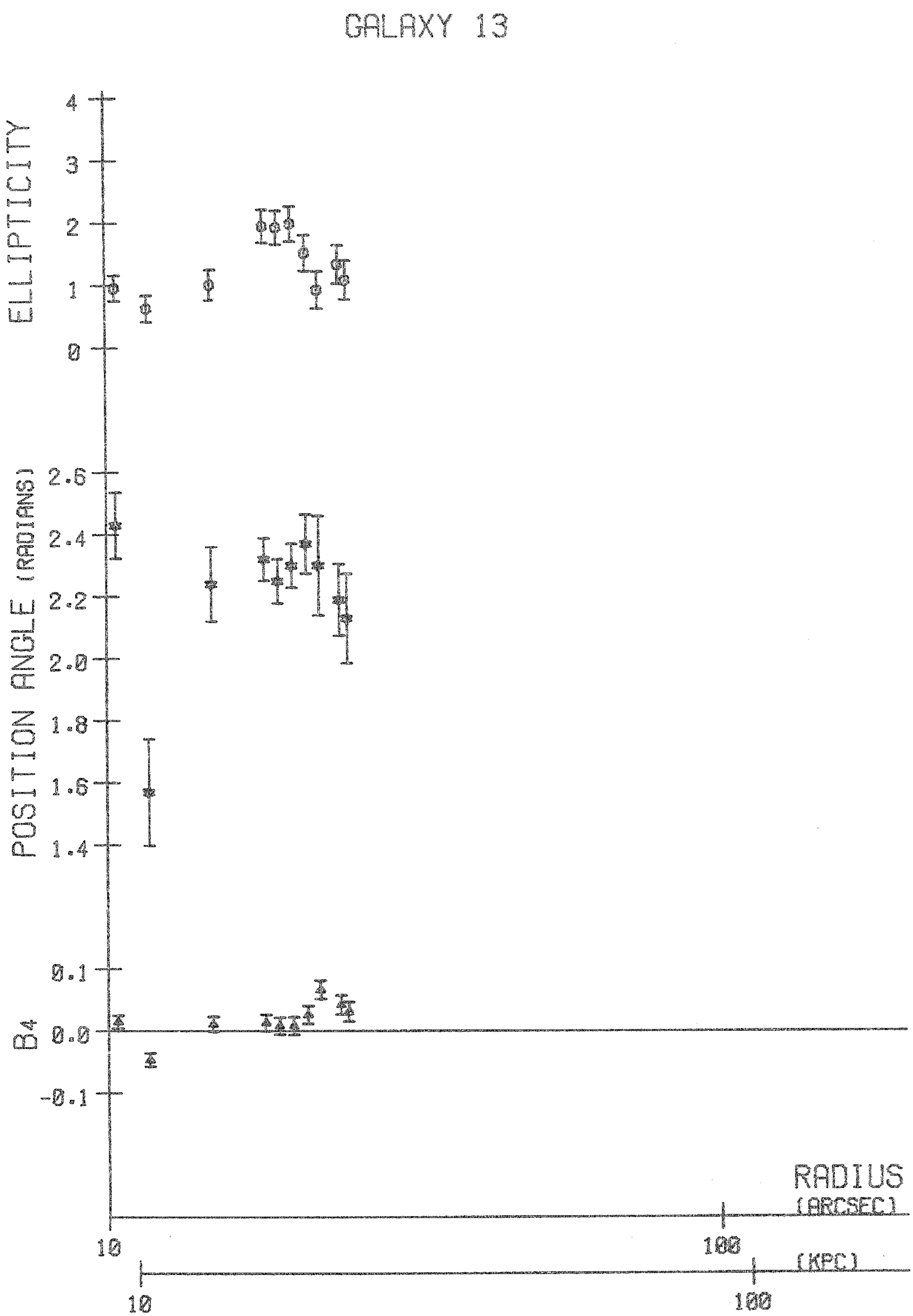

D13 Figure 14 – ε, θ, and B_4 against radius for galaxy 13.

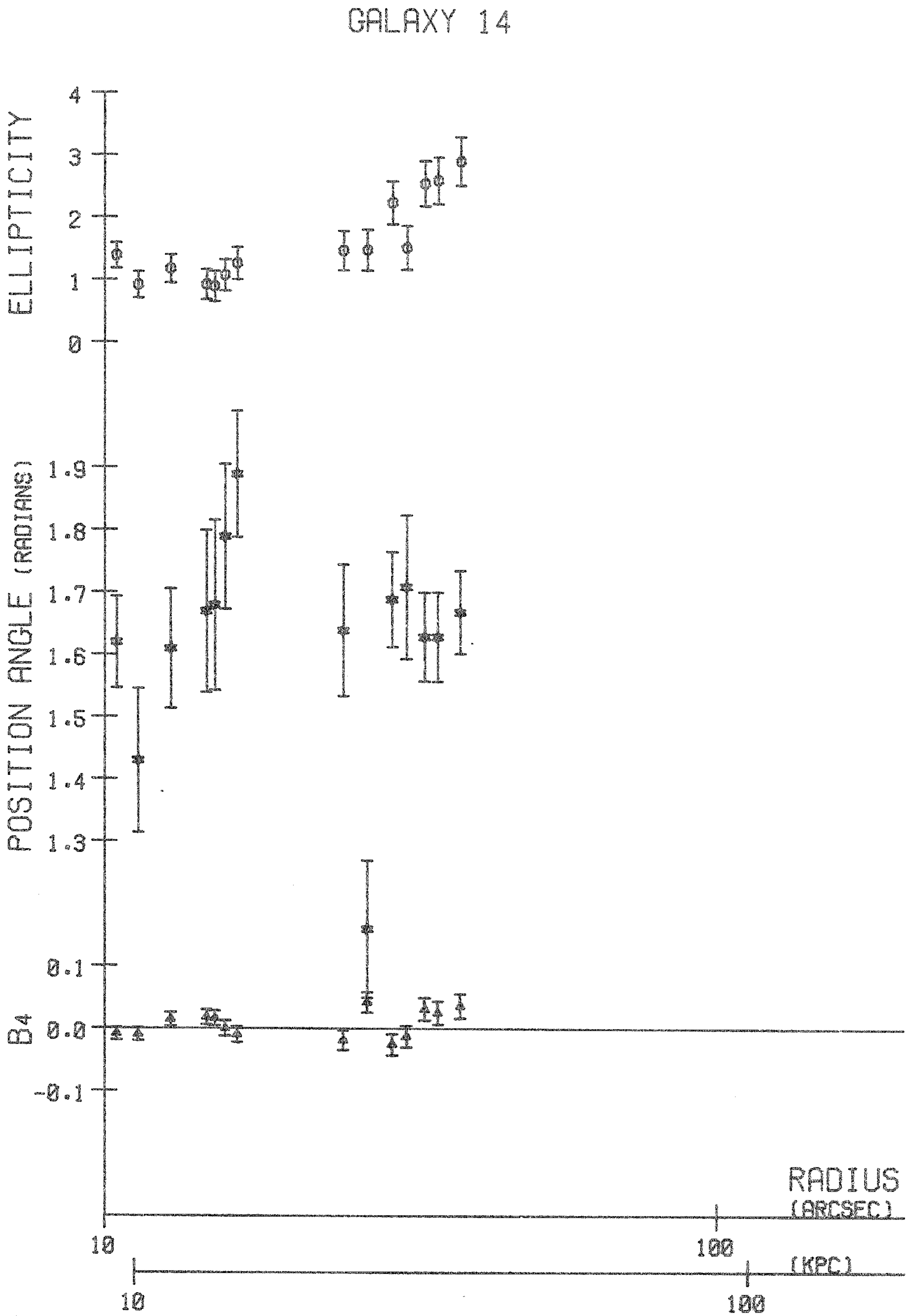

D14 Figure 15 - ε, θ, and B_4 against radius for galaxy 14.

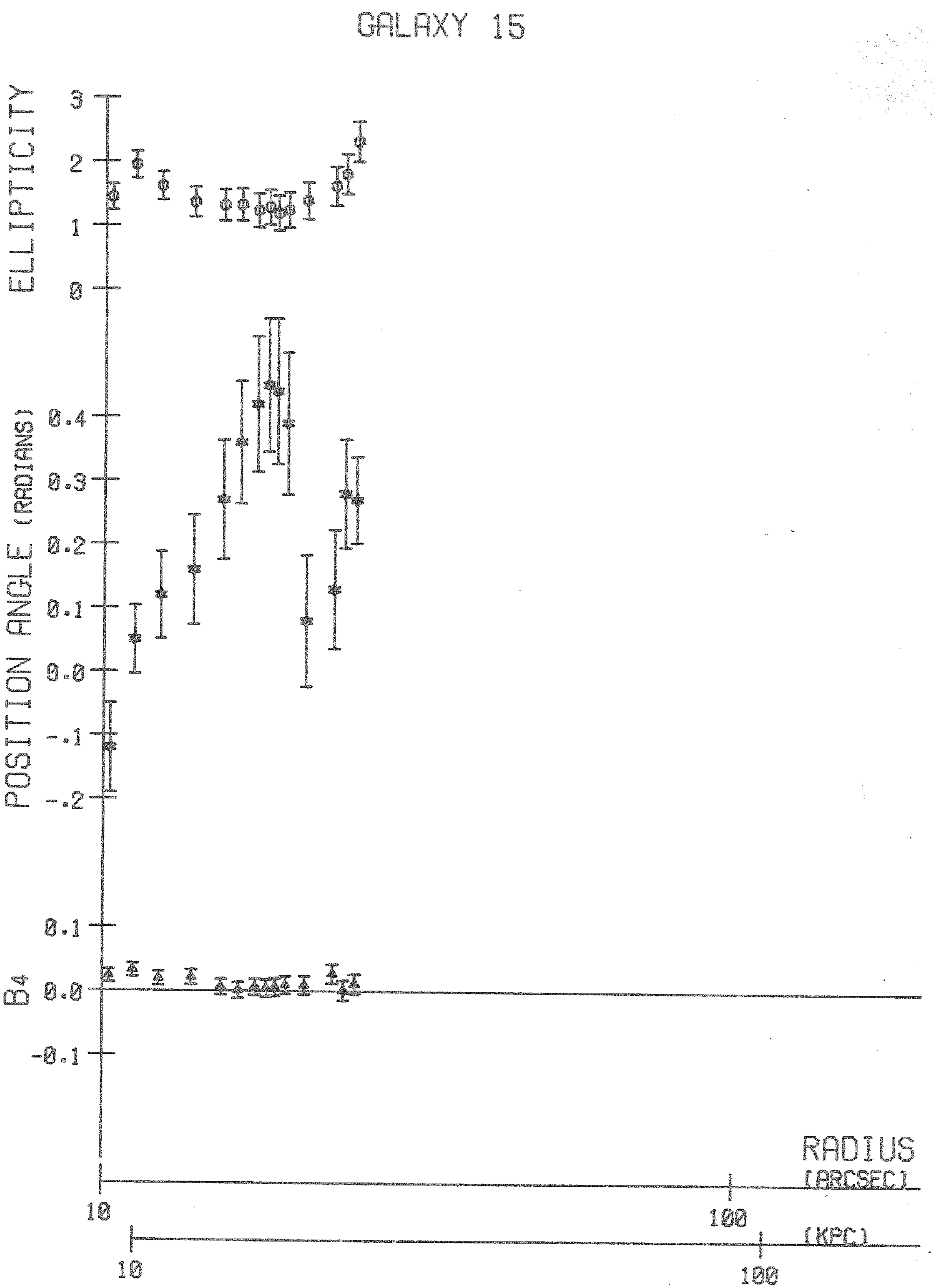

E01 Figure 16 - ε, θ, and B_4 against radius for galaxy 15.

4. Accuracy and Significance of the results

A. Comment on the major sources of error

Three sources contribute to the noise in the data: the photographic plate, the microdensitometer and the sky. Although the calibration of the plate is somewhat uncertain at high densities this does not affect the measurements presented here, as the surface brightnesses of the isophotes are not used. Assuming that the density range of the microdensitometer is 0-4D the range of densities over which the isophotes used occur is 0.4 - 2.0D. The density gradients involved are small, the largest, in the centre of NGC 6166, is 0.3D/resolution element (15 microns), and at these density gradients both the effect of transmission smoothing by the microdensitometer and that of adjacency effects in the photographic emulsion are small ($\lesssim$ 1%).

Laboratory tests (Miller 1971) and examination of star profiles from the plate used in this study (Carter 1977b) and those used in other photometric studies (Godwin 1976) show no significant density gradient dependent effects at the densities and density gradients in question. Comparison with results from another IIIaJ plate scanned at 25 micron resultion (K.L. Dixon; private communication) shows that the resolution does not significantly affect the results in the centres of the objects. Most of the resolution problems come from the point source response function (seeing profile), and an attempt is made to correct for this. At densities of about 3.0D a time constant in the microdensitometer is apparent, but such densities are not reached in this study.

The most serious source of error is the contamination due to residual star images and particularly the haloes of other nearby galaxies. This affects the outer regions of the images, causing scatter in the points in Figures 2 - 16. It seems that these effects will not be systematic.

B. Comparison with results from another plate

Figures 17 - 21 show the results derived by the same techniques from a deep red (127 - 04 + RG1) plate of the same region of the sky, loaned by Dr. J.V. Peach and Dr. J.G. Godwin. No colour gradients are present in the outer regions of these galaxies, so the difference in the waveband should have no effect. The diagrams are for galaxies 1, 2, 3, 4 and 6. Comparison with Figures 2 - 5 and 7 shows that the basic features of the ellipticity and orientation profiles are the same. Differences in the outermost parts are due to the slightly different effect of the treatment of overlapping objects, the images on the red plate are slightly larger than on the IIIaJ plate.

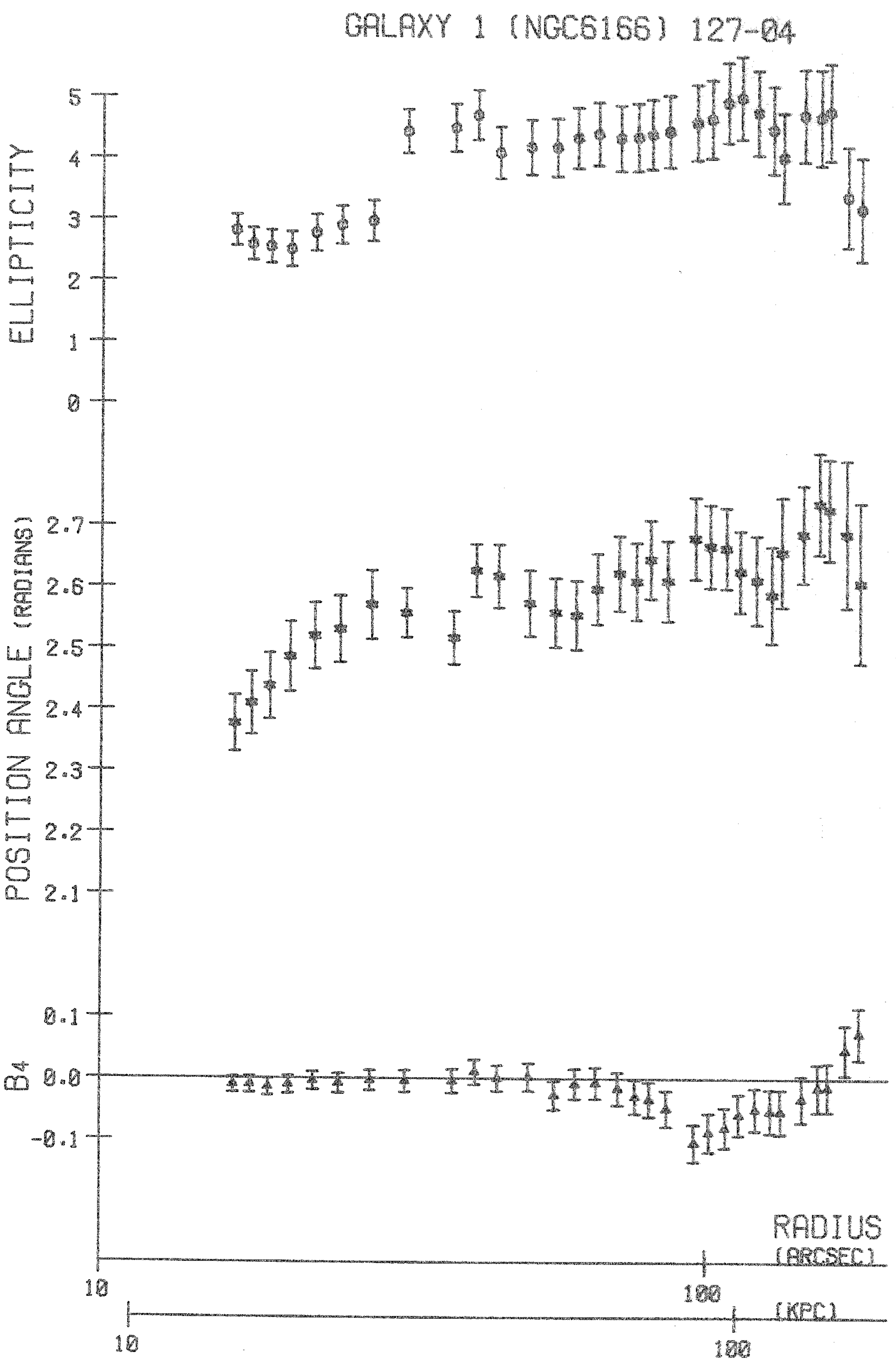

E03 Figure 17 - ε, θ, and B_4 against radius for galaxy 1 from deep red (127-04) plate.

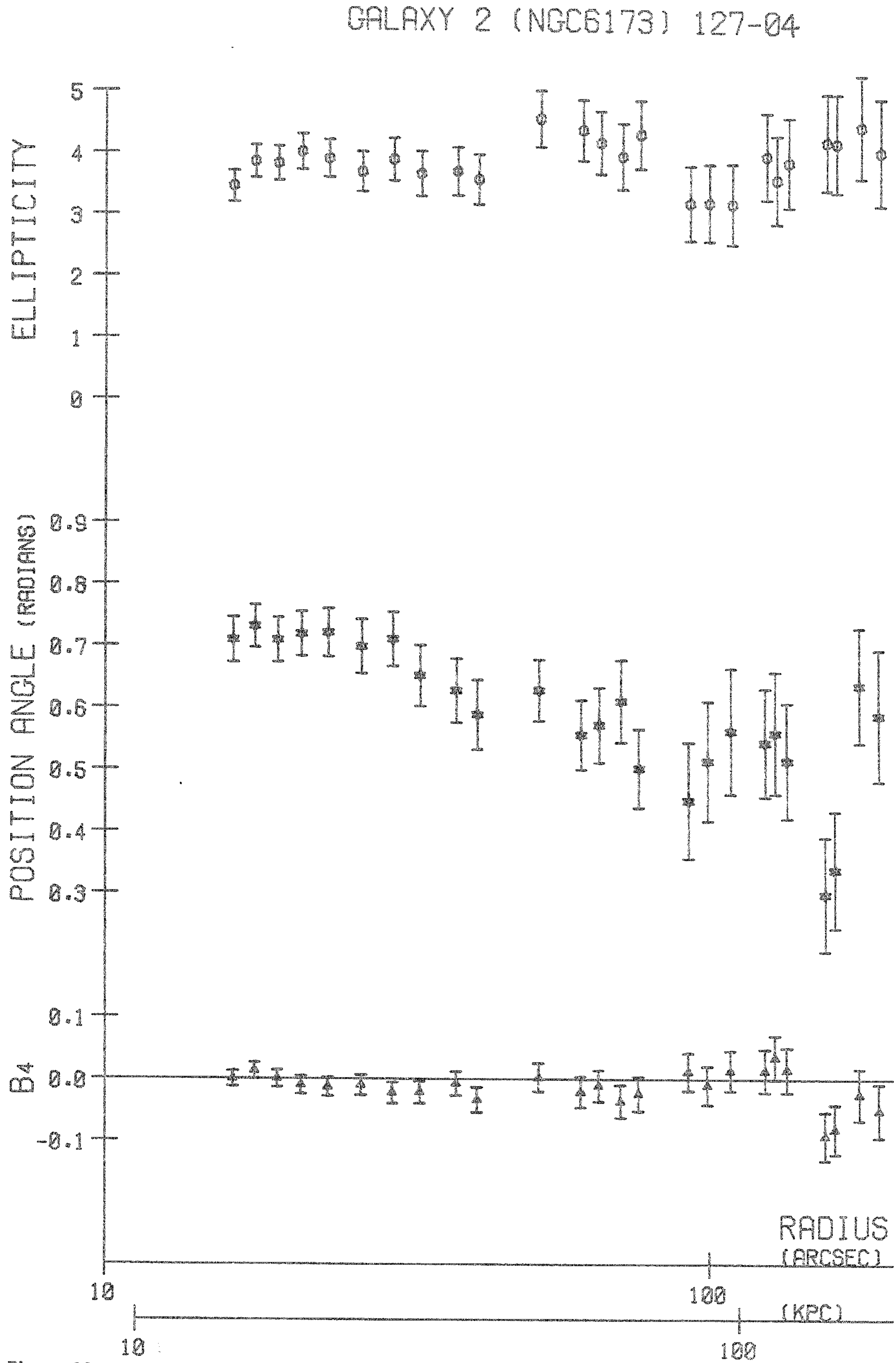

E04 Figure 18 - ε, θ, and B_4 against radius for galaxy 2 from 127-04 plates.

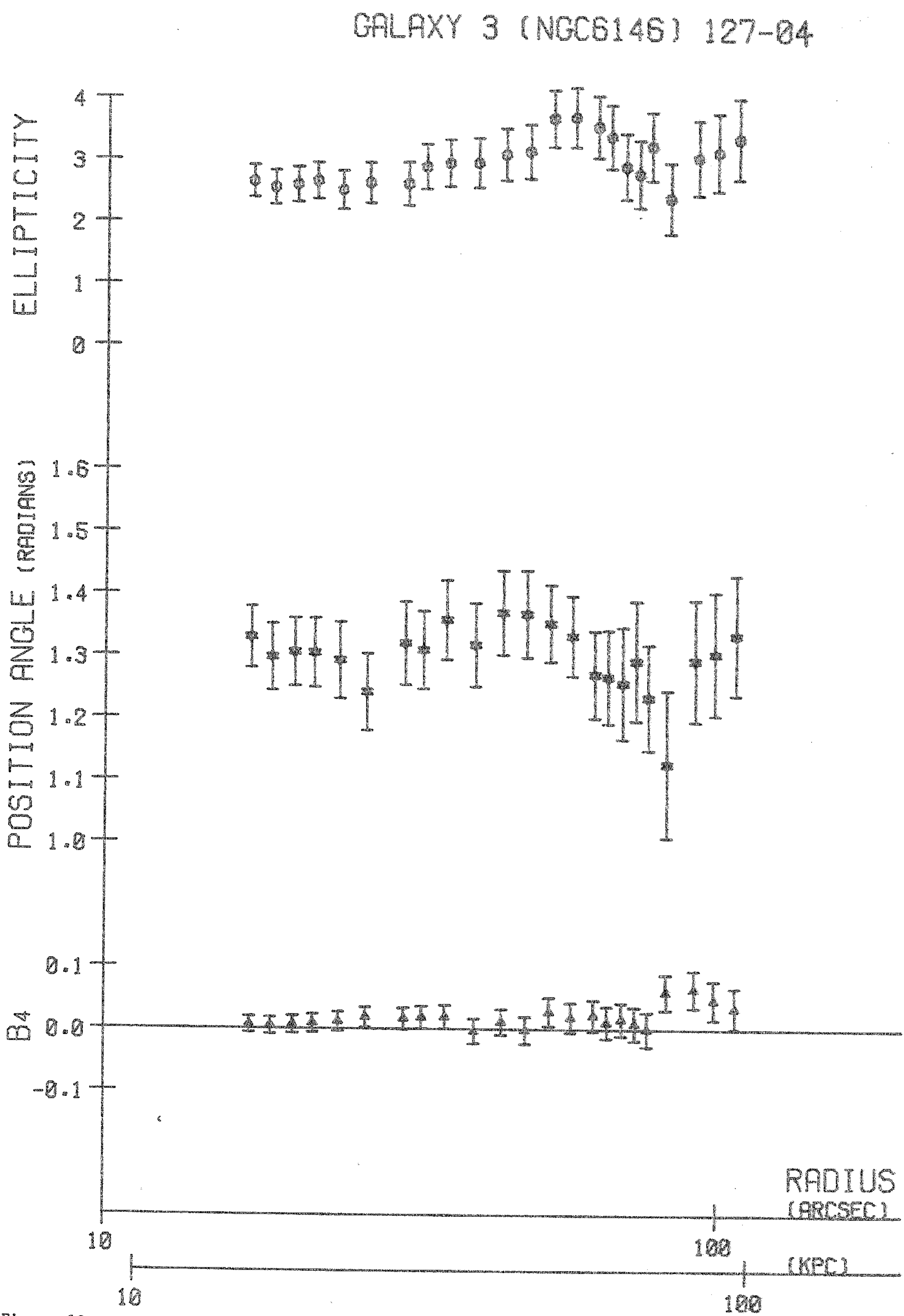

E05 Figure 19 – ε, θ, and B_4 against radius for galaxy 3 from 127-04 plate.

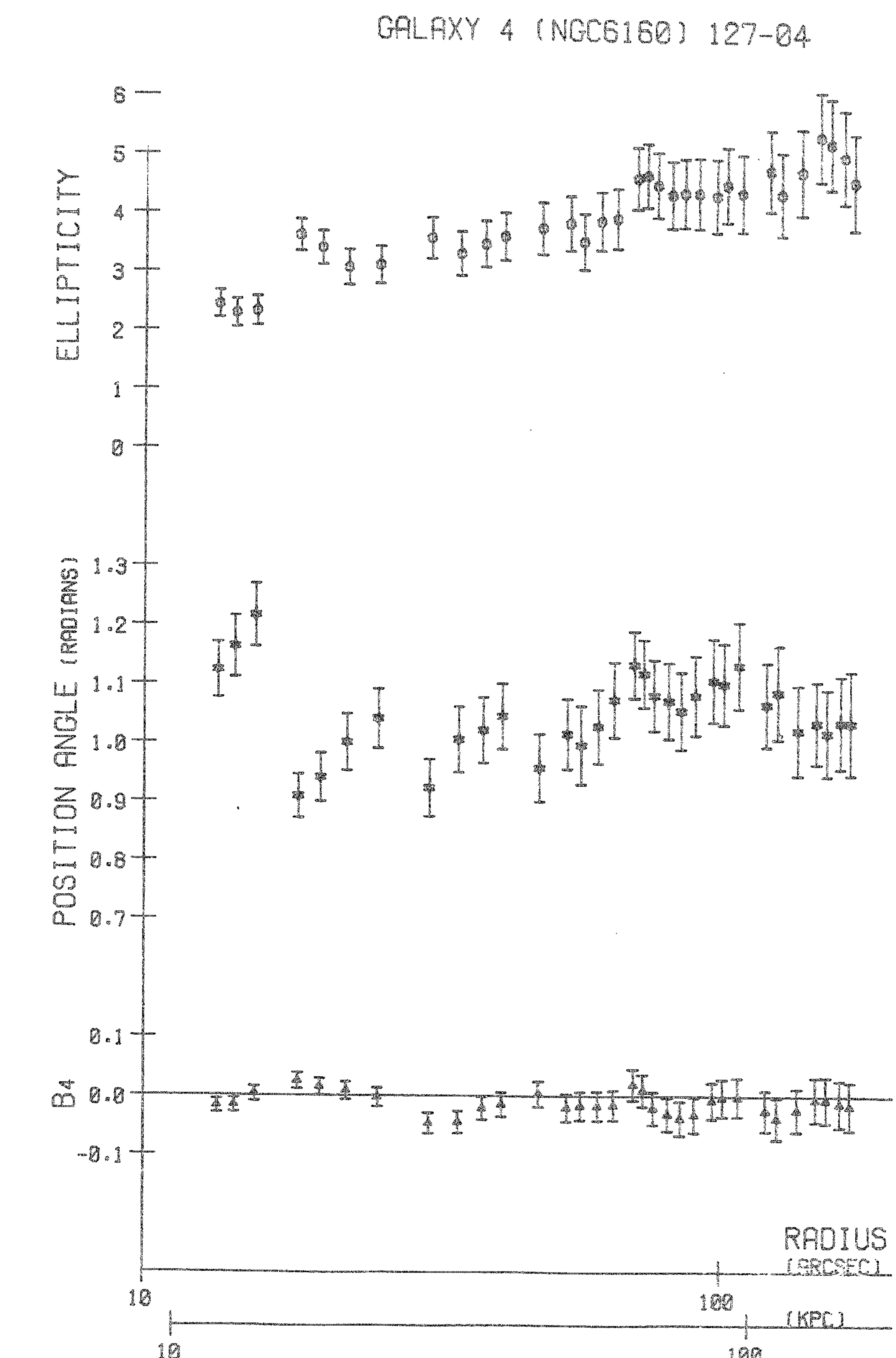

E06. Figure 20 - ε, θ, and B_4 against radius for galaxy 4 from 127-04 plate.

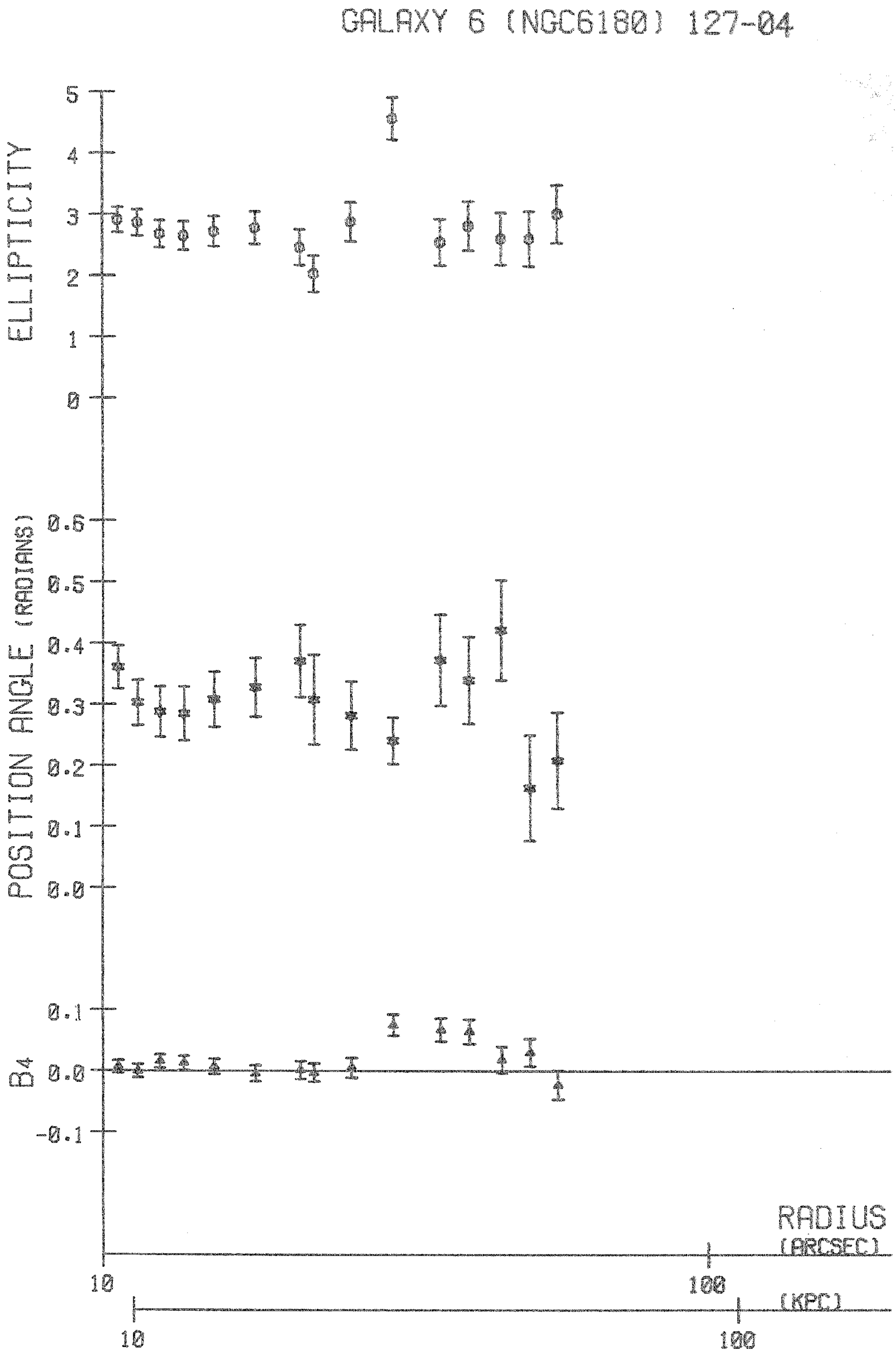

E07 Figure 21 - ε, θ, and B_4 against radius for galaxy 6 from 127-04 plate.

As this plate is slightly more exposed, some points at smaller radii are not used, as they are affected by errors in the microdensitometer at high densities. The non-zero values of B_4 still appear not to be significant. These results tend to confirm the conclusion that the results are not particularly sensitive to photographic effects, but do not rule out the possibility that errors intrinsic to the sky affect the results. Values of ε are corrected for a gaussian point spread function of standard deviation 2.8 arcsec.

C. Detailed analysis of the data on galaxy 1

Figure 22 shows some of the isophotes used together with the fitted ellipses, both before and after correction for non-zero A_0. These diagrams illustrate the effects of the haloes of other galaxies on the isophotes. In Figure 22(a) the isophotes are systematically too large, in Figure 22(b) they have been corrected for non-zero A_0, but the ellipses are affected by the distortions caused by the fainter galaxies. The distortions cause scatter in the points, but it seems that they will not cause systematic errors. A number of objects have been removed from these maps, and only the faint outer haloes of the galaxies remain.

For each contour of NGC 6166 a closeness of fit parameter was determined by computing the sum

$$\xi = \frac{\sum_i [R_i - 1]^2}{n} ,$$

where n is the total number of points, after R_i had been corrected for the non-zero value of $(A_0 - 1)$.

ξ is not a formal χ^2 value, in this case the χ^2 statistic is not very meaningful, as $(R_i - 1)$ is not normally distributed due to the fact that adjacent points are not necessarily uncorrelated. Only if the point spread function is a delta function, and star images are simply points is it possible to work out a meaningful χ^2 value. In this case noise due to the residues of images of bright foreground stars dominates over noise due to faint foreground stars and due to photon statistics.

Table 2 gives values of ξ for a number of contours of galaxy 1. This table also gives uncorrected values of R and all Fourier components up to the fourth order, and corrected values of ε and θ. From the values of ξ in Table 2 we can see that the fit gradually gets worse as R increases.

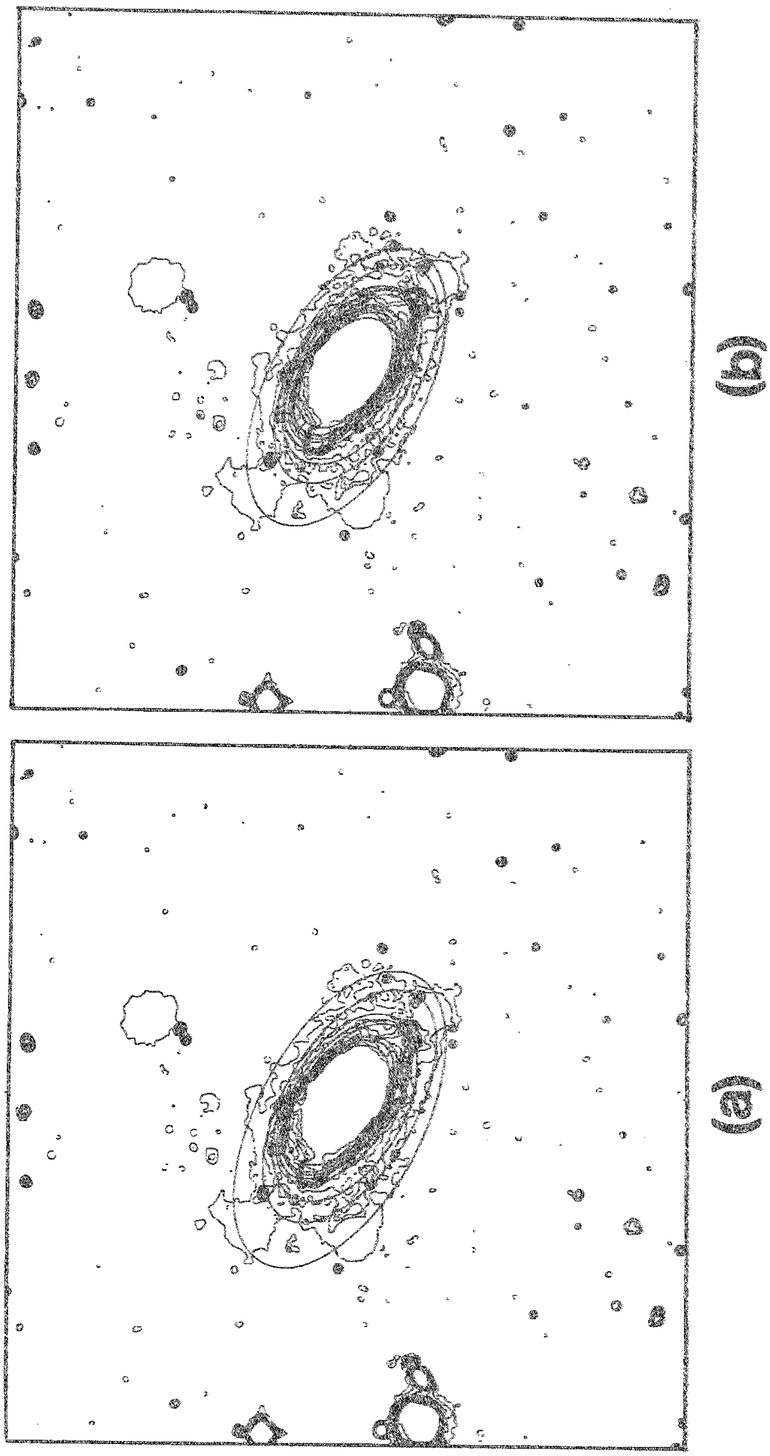

Figure 22 - Shapes of isophotes and the fitted ellipses for the outer parts of galaxy 1. (a) Before correction of the fitted ellipses for non zero A_O. (b) After correction for non zero A_O.

TABLE 2 - FOURIER COMPONENTS AND GOODNESS OF FIT PARAMETER FOR GALAXY 1

R	ε	θ	ξ	A_0	A_1	B_1	A_2	B_2	A_3	B_3	A_4	B_4
10.40	3.55	2.20	0.0019	0.9930	-0.0220	-0.0060	-0.0030	0.0008	-0.0415	-0.0089	0.0045	0.0030
11.12	3.49	2.24	0.0013	0.9946	0.0022	-0.0041	0.0011	-0.0031	0.0395	-0.0022	0.0058	0.0002
11.97	3.26	2.27	0.0010	0.9965	0.0017	-0.0002	-0.0007	0.0011	0.0354	-0.0016	-0.0044	-0.0053
13.08	3.13	2.28	0.0014	0.9972	0.0025	0.0012	0.0052	-0.0026	0.0352	-0.0061	0.0008	-0.0109
13.86	2.93	2.31	0.0016	0.9910	0.0012	-0.0019	0.0006	-0.0009	0.0375	0.0063	0.0044	-0.0134
14.55	2.99	2.33	0.0015	0.9950	0.0005	0.0035	0.0019	-0.0021	0.0371	0.0137	0.0046	-0.0139
15.49	2.95	2.38	0.0020	0.9920	0.0053	0.0027	-0.0043	0.0004	0.0427	0.0194	-0.0064	-0.0153
16.50	2.90	2.39	0.0015	0.9940	-0.0014	0.0009	-0.0015	-0.0022	0.0355	0.0180	-0.0055	-0.0176
17.66	2.72	2.40	0.0013	0.9960	0.0008	0.0015	-0.0015	-0.0009	0.0305	0.0184	-0.0024	-0.0172
19.19	2.58	2.44	0.0012	0.9960	-0.0014	0.0003	-0.0005	-0.0001	0.0280	0.0158	-0.0005	-0.0152
20.03	2.57	2.47	0.0016	0.9940	0.0007	0.0019	-0.0018	-0.0007	0.0206	0.0203	-0.0006	-0.0164
20.95	2.60	2.48	0.0016	0.9950	0.0011	-0.0014	-0.0004	-0.0014	0.0182	0.0184	0.0039	-0.0159
21.86	2.62	2.49	0.0015	0.9980	0.0007	0.0052	0.0029	-0.0018	0.0129	0.0130	0.0095	-0.0186
23.07	2.74	2.51	0.0012	0.9980	0.0020	0.0020	0.0013	-0.0034	0.0105	0.0104	0.0114	-0.0135
24.46	2.81	2.49	0.0014	0.9940	-0.0015	0.0009	0.0021	-0.0011	0.0169	0.0133	0.0082	-0.0105
26.35	2.69	2.48	0.0021	0.9930	0.0018	-0.0007	-0.0003	0.0014	0.0175	0.0190	0.0066	-0.0115
28.51	2.96	2.49	0.0024	0.9960	0.0007	0.0037	0.0006	-0.0016	0.0084	0.0230	0.0161	-0.0087
31.46	3.06	2.46	0.0028	0.9850	-0.0019	0.0097	0.0118	0.0008	-0.0002	0.0219	0.0132	-0.0147
35.16	3.54	2.51	0.0028	0.9880	-0.0046	0.0011	-0.0005	-0.0004	-0.0012	0.0205	0.0112	0.0045
42.34	4.41	2.61	0.0096	0.9590	-0.0164	-0.0272	-0.0319	-0.0272	0.0163	0.0279	0.0391	0.0120
52.90	4.81	2.48	0.0123	0.9520	0.0088	-0.0027	0.0310	-0.0307	0.0649	-0.0321	0.0312	-0.0133
56.31	4.75	2.52	0.0090	0.9770	0.0006	0.0252	0.0048	-0.0006	0.0690	-0.0306	-0.0086	0.0052
62.58	4.47	2.58	0.0098	0.9670	-0.0241	-0.0205	-0.0224	0.0032	0.0400	-0.0274	-0.0289	-0.0221
66.82	4.26	2.59	0.0107	0.9630	-0.0181	-0.0123	0.0012	0.0033	0.0330	-0.0623	-0.0493	-0.0359
80.72	4.61	2.59	0.0205	0.9330	0.0522	0.0154	0.0048	0.0276	-0.0706	0.0960	-0.0787	-0.0382
87.18	4.42	2.68	0.0186	0.9400	0.0100	-0.0072	-0.0395	0.0129	-0.0714	0.0284	-0.0466	-0.0899
100.10	4.87	2.61	0.0200	0.9490	-0.0071	-0.0308	-0.0024	-0.0044	-0.0063	-0.0682	-0.1190	-0.0413
111.30	4.62	2.62	0.0177	0.9460	-0.0057	-0.0390	0.0005	0.0063	-0.0374	-0.0483	-0.0828	-0.0443
125.02	3.98	2.56	0.0214	0.9370	-0.0118	0.0147	0.0043	0.0409	-0.0365	-0.0852	-0.0300	-0.0138
136.90	3.50	2.61	0.0194	0.9420	-0.0006	-0.0112	0.0026	0.0649	-0.0258	-0.0888	-0.0233	-0.0212
144.71	4.02	2.65	0.0178	0.9430	0.0244	-0.0082	-0.0044	0.0294	0.0072	-0.0821	-0.0045	-0.0275
156.06	3.90	2.61	0.0149	0.9440	0.0026	0.0070	0.0175	0.0272	-0.0080	-0.0639	0.0050	-0.0324
174.88	4.49	2.66	0.0175	0.9410	-0.0126	-0.0362	-0.0023	0.0064	0.0416	0.0274	0.0360	-0.0407

5. Discussion

A. Comparison with other observational results

The trend for ellipticity to increase with radius in elliptical galaxies has been known for some time. Redman and Shirley (1938) found that ellipticity was not constant with radius, but did not present ellipticity profiles. In an early photographic study of Virgo cluster galaxies Liller (1960, 1966) showed that ellipticals have increasing or peaked ellipticity profiles, and inspection of the tables in these two papers shows some evidence of variations of position angle with radius, although the significance of this is difficult to assess. Detailed studies of nearby dwarf ellipticals (Hodge 1963, 1973, 1976) show ellipticity to be an increasing function of radius there. Arp and Bertola (1969) showed that the outermost isophotes of M87 were elongated, and a detailed study of M87 (Carter and Dixon 1977) has shown that the form of the ellipticity profile of this galaxy is somewhat similar to those presented for the brighter ellipticals here, although ellipticity is a stronger function of radius in M87. No evidence is found for variation of the position angle with radius in M87.

Barbon, Capaccioli and Tarenghi (1975) and Barbon and Cappaccioli (1975) showed ellipticity increasing with radius in two SB0 galaxies. Barbon, Benacchio and Capaccioli (1976) made a photometric study of three galaxies including the bright elliptical NGC 3379, which unfortunately did not go very deep. They showed ellipticity increasing weakly with radius, and also plotted the position angle of the major axis and the positions of the centres of the isophotes, although these data are somewhat inconclusive. A comparison of the techniques used by Barbon, Benacchio and Capaccioli with those used here would be of interest, but unfortunately Barbon et al say very little about their techniques or the quality of their observational material.

I.R. King (private communication) has shown ellipticity to be a monotonically increasing function of radius in several Virgo cluster ellipticals, and is also reported to have found significant variations of position angle with radius.

B. Comparison with theoretical predictions

The models of elliptical galaxies which have been published divide into two types. Those of Prendergast and Tomer (1970), and Wilson (1975) are based on finding steady state solutions of the non-linear Poisson equation:

$$\nabla^2 U(\underline{r}) = 4\pi G\rho(\underline{r}, U) ,$$

$$\rho(\underline{r}, U) = \iiint_{-\infty}^{\infty} F(E, J)\, d^3\underline{v} ,$$

where $E = \frac{1}{2}v^2 + U(r)$ is the total energy, $J = r \sin\theta\, v_\phi$ is the angular momentum, $U(r)$ is the gravitational potential, d^3v refers to integration over velocity space and $F(E, J)$ is the stellar distribution function.

Prendergast and Tomer used:

$$F(E, J) = e^{-E+\beta J} \qquad E \le 0 ,$$
$$= 0 \qquad E > 0 ,$$

which has a somewhat unrealistic discontinuity at $E = 0$.

The models produced has a realistic run of density with radius. The ellipticity profiles however were somewhat more strongly peaked than the observational profiles. ϵ would typically rise from 1 to as much as 4, and then decrease back down to 1. Although they did not carry out Fourier analysis of their isophotes, inspection of their Figure 3 suggests that the isophotes of moderately flattened models tend to be box-shaped, i.e. to have negative B_4, especially at large radius.

Wilson used the distribution function:

$$F(E, J) = (e^{-E} - 1 + E) \exp(\beta J - \tfrac{1}{2}\xi^2 J^2), \qquad E \le 0 ,$$
$$= 0 \qquad E > 0 .$$

His extra free parameter, ξ, enabled him to treat differential rotation independently of the energy cutoff. His ellipticity profiles were also strongly peaked, he compared them with measurements of the ellipticity profile of NGC 3379, based on the surface photometry of Miller and Prendergast (1962), and on his own measurements from photographs by Dennison and by Hodge. He found that the ellipticity profile of NGC 3379 was much less sharply peaked than those of his models, as found for the present galaxies. From Fourier analysis of his isophotes he concluded that deviations from ellipticity were small.

The models of Wilson and of Prendergast and Tomer were constructed to fit NGC 3379, but should scale simply to larger and more massive galaxies such as NGC 6166 and NGC 6173.

The second class of models includes those of Larson (1975) and Gott (1975). Larson considers the collapse of a cloud of gas with star formation taking place during the collapse phase. Larson's models are again computed to fit NGC 3379, and the scaling to larger and more massive galaxies is not so simple here. It is difficult to see what effect this scaling would have on the general properties of the models. Larson's ellipticity profiles are similar to those of Wilson, although those with a high turbulent viscosity are less strongly peaked, and resemble the observations more closely.

Gott (1975) considers a situation where the star formation process is complete before the collapse begins, so he is dealing with the collapse of a cloud of stars. His models show ellipticity decreasing with radius, which is not in agreement with the observations. This could be because in Gott's model violent relaxation is only taken into account in a radial direction, and azimuthal violent relaxation is not allowed for, (B.J. T. Jones, private communication).

Lynden-Bell (1967) showed that the form of the distribution function depended upon the third integral of motion, and showed in an asymptotic approximation that the ellipticity of the isophotes tends to a constant value at large radius. No calculations have yet been carried out with the form of the distribution function found by Lynden-Bell. The theory of the violent relaxation of rotating systems is not sufficiently rigorous to pin down the exact form of the distribution function. Further calculations are necessary here.

A completely different interpretation of the flattening of elliptical galaxies is discussed by Binney (1976). He considers the violent relaxation of a sheet of stars, the sheet having been formed after the anisotropic collapse of a cloud of gas. He found that violent relaxation of the sheet led to the formation of a flattened equilibrium system, resembling an elliptical galaxy, whether or not the sheet was rotating. The advantage of this model is that it leads to a more realistic frequency distribution of ellipticity than that found for simple dissipationless collapse (Thuan and Gott, 1975). Binney's numerical calculations involved considering a system of only about 200 mass points, so further calculations are necessary before it can be seen whether this model predicts ellipticity distributions in agreement with those observed.

The variation of position angle with radius seems to be a real feature, and is clearly not accounted for in simple models with an axis of symmetry. It seems that there are two plausible explanations for this effect.

(1) The outer regions of elliptical galaxies are not in fact relaxed; this could be due to one of three reasons: material may have fallen into the halo of the galaxy and not yet reached an equilibrium state, or the galaxy may have been disturbed by an encounter with another object, or the outer parts may not have been relaxed when the galaxy formed.

(2) The galaxy could be in a triaxial equilibrium state, when it appears that the projected distribution could have a form where the major axes of the isophotes were not all of the same position angle (c.f. Stark (1977) on the nuclear bulge of M31).

The observations presented here fit the models of Larson reasonably well, particularly those models in which the star formation is completed during the early phases of the collapse of the galaxies, and those in which the turbulent viscosity is high. The observations fit in reasonably well with the steady state models of Wilson, but the difficulty mentioned by Wilson still remains in that the ellipticity profiles of the models are still more strongly peaked than the observations. Further work in progress on the models of Binney should indicate whether these models fit the observations satisfactorily.

6. The displacement of the centres of the isophotes

The ellipse fitting procedure produces two more parameters to describe the best fit ellipse to each isophote, they are x_0 and y_0 in equation 1, which define the centre of the ellipse. For only two galaxies did these differ significantly between the innermost and outermost isophotes. These were the two brightest galaxies, NGC 6166 and NGC 6173.

In NGC 6166 the centre is displaced in a southerly direction in the outermost parts by up to 20 arcsec. The multiple nucleus structure of this galaxy (Minkowski 1961) has a scale of about 10 arcsec, and only affects the very innermost isophotes used in this analysis. The second brightest nucleus is approximately WNW of the brightest, and the third brightest is almost due west.

At the distance of 186 Mpc assumed for these galaxies 1 arcsec is 0.9 kpc.

In NGC 6173 the centre in the outer parts is displaced along the major axis in a south-easterly direction, which is away from the rest of the cluster. The maximum displacement is again of order 20 arcsec.

One effect which could cause apparent displacement of the centres of the isophotes would be a sloping sky background or emulsion sensitivity across the image. However the maximum slope which would be consistent with the shapes of the radial profiles observed (Carter 1977a) would be 1/2% across the image. This would give rise to a displacement of up to 5 arcsec for the outer isophotes. As the observed displacement is 20 arcsec it seems that this error does not account for all of the effect. Another possible error in these data is the contamination due to the haloes of other galaxies. It seems unlikely that this could entirely account for the effect, especially in the case of NGC 6173, where there are not quite so many nearby objects. Further measurements on cD galaxies, and an improvement in the techniques of handling overlapping light distributions are required before a final verdict on the reality of this effect can be given. The cause of the asymmetry, if real, is not clear, it may be due to interactions with other galaxies, although tidal interactions would be expected to give quadrupole distortions (B.J.T. Jones, private communication). Sufficiently large quadrupole distortions are not observed. The asymmetry might alternatively be due to accretion onto the supergiant galaxy of material from other galaxies (Richstone 1976), which could be somewhat anisotropic.

Acknowledgements

I thank C.D. Mackay, D. Lynden-Bell and B.J.T. Jones for many helpful discussions on the subject of this paper, and for comments on the manuscript. I thank Professor I.R. King and an anonymous referee for comments on the original draft of this paper. I thank Dr. Jon Godwin for comments and for providing several references. The method of Fourier analysis of the isophotes of galaxies was suggested to me by E.J. Kibblewhite. The loan of the plates by C.D. Mackay and R.J.E. Kraft, and by J.V. Peach and J.G. Godwin is gratefully acknowledged. I thank G.E.M. Jared for assistance with the computing and J. Pilkington and K.F. Hartley for assistance with the PDS microdensitometer. I acknowledge an S.R.C. studentship whilst the first part of this work was carried out.

References

Arp, H.C., and Bertola, F., 1969, Astrophys.Lett., 4, 23.

Barbon, R., Capaccioli, M., & Tarenghi, M., 1975, Astr.Astrophys., 38, 315.

Barbon, R., and Capaccioli, M., 1975, Astr.Astrophys., 42, 103.

Barbon, R., Benacchio, L., & Capaccioli, M., 1976, Astr.Astrophys., 51, 25.

Binney, J.J., 1976, Mon.Not.R.Astr.Soc., 177, 19.

Carter, D., 1977a, Mon.Not.R.Astr.Soc., 178, 137.

Carter, D., 1977b, Thesis, Cambridge University.

Carter, D., and Dixon, K.L., 1977, Submitted to Astron.J.

Godwin, J.G., 1976, Thesis, Oxford University.

Gott, J.R., 1975, Astrophys. J., 201, 296.

Hodge, P.W., 1963, Astron.J., 68, 691.

Hodge, P.W., 1973, Astrophys.J., 182, 671.

Hodge, P.W., 1976, Astron.J., 81, 25.

Hoffman, A.W., and Crane, P., 1977, Astrophys.J., 215, 379.

Kibblewhite, E.J., 1969, Thesis, Cambridge University.

Larson, R.B., 1975, Mon.Not.R.Astr.Soc., 173, 671.

Liller, M.H., 1960, Astrophys.J., 132, 306.

Liller, M.H., 1966, Astrophys.J., 146, 28.

Lynden-Bell, D., 1967, Mon.Not.R.Astr.Soc., 136, 101.

Miller, R.H., and Prendergast, K.H., 1962, Astrophys.J., 136, 713.

Miller, W.C., 1971, A.A.S. Photo-Bulletin No.2, p3.

Prendergast, K.H., and Tomer, E., 1970, Astron.J., 75, 674.

Redman, R.O., and Shirley, W.G., 1938, Mon.Not.R.Astr.Soc., 98, 613.

Richstone, D.O., 1976, Astrophys.J., 204, 642.

Rood, H.J., and Sastry, G., 1972, Astron.J., 77, 451.

Stark, A.A., 1977, Astrophys.J., 213, 368.

Wilson, C.P., 1975, Astron.J., 80, 175.

Zwicky, F., 1973; Catalogue of selected compact and post-eruptive galaxies, F. Zwicky.

Zwicky, F., and Herzog, E., 1966, Catalogue of galaxies and clusters of galaxies, Vol.III, Caltech.

APPENDIX A

Data are presented here in tabular form for 4 of the galaxies in Table 1. In each of Tables 3 - 6 column 1 is the corrected value of the average radius of the isophote, column 2 the ellipticity and column 3 the position angle in radians measured with respect to the North-South direction. For galaxies 1, 2 and 11 this is positive in a clockwise sense, and for galaxy 5 it is positive in an anticlockwise sense. Columns 4 and 5 give the displacement of the centre of the isophote relative to the centre at a radius of 10 arcsec. These displacements are transformed such that x_0 is along the major axis and y_0 along the minor axis. Columns 6 - 14 give the first eight Fourier components. They are corrected for non zero A_0, the correction in most cases is small.

Distortion of isophotes by a single star will often show up as a large third order Fourier component (either A_3 or B_3). Non-zero values of first and second order components are due to inaccuracies in the fitting method, and are also an indication of distortion by some object. Fourth order Fourier components, particularly B_4, show the deviations of the isophote from ellipticity.

F03

TABLE 3 - GALAXY 1 (NGC 6166)

R	ε	θ	x_0	y_0	A_1	B_1	A_2	B_2	A_3	B_3	A_4	B_4
10.33	3.55	2.20	0.0	0.0	-0.0222	-0.0060	-0.0030	0.0008	0.0418	-0.0090	0.0045	0.0030
11.06	3.49	2.24	0.14	0.06	0.0022	-0.0041	0.0011	0.0031	0.0397	-0.0022	0.0058	0.0002
11.92	3.26	2.27	0.24	0.16	0.0017	-0.0002	-0.0007	0.0011	0.0355	-0.0016	-0.0044	-0.0053
13.04	3.13	2.28	0.46	0.24	0.0025	0.0012	0.0052	-0.0026	0.0353	-0.0061	0.0008	-0.0109
13.74	2.93	2.31	0.56	0.23	0.0012	-0.0019	0.0006	-0.0009	0.0378	0.0064	0.0044	-0.0135
14.48	2.99	2.33	0.55	0.23	0.0005	0.0035	0.0019	-0.0021	0.0373	0.0138	0.0046	-0.0140
15.37	2.95	2.38	0.74	0.31	0.0053	0.0027	-0.0043	0.0004	0.0430	0.0196	-0.0065	-0.0154
16.40	2.90	2.39	1.00	0.30	-0.0014	0.0009	-0.0015	-0.0022	0.0357	0.0181	-0.0055	-0.0177
17.59	2.72	2.40	1.20	0.33	0.0008	0.0015	-0.0015	-0.0009	0.0306	0.0185	-0.0024	-0.0173
19.11	2.58	2.44	1.50	0.18	-0.0014	0.0003	-0.0005	-0.0001	0.0281	0.0159	-0.0005	-0.0153
19.91	2.57	2.47	1.57	0.15	0.0007	0.0019	-0.0018	-0.0007	0.0207	0.0204	-0.0006	-0.0165
20.84	2.60	2.48	1.83	0.09	0.0011	-0.0014	-0.0004	-0.0014	0.0183	0.0185	0.0039	-0.0160
21.82	2.62	2.49	1.63	0.25	0.0007	0.0052	0.0029	-0.0018	0.0129	0.0130	0.0095	-0.0186
23.03	2.74	2.51	1.89	0.30	0.0020	0.0020	0.0013	-0.0034	0.0105	0.0104	0.0114	-0.0135
24.31	2.81	2.49	2.14	0.21	-0.0015	0.0009	0.0021	-0.0011	0.0170	0.0134	0.0082	-0.0106
26.17	2.69	2.48	1.81	0.14	0.0018	-0.0007	-0.0003	0.0014	0.0176	0.0191	0.0066	-0.0116
28.40	2.96	2.49	1.97	0.13	0.0007	0.0037	0.0006	-0.0016	0.0084	0.0231	0.0162	-0.0087
30.99	3.06	2.46	2.33	-0.45	-0.0019	0.0098	0.0120	0.0008	-0.0002	0.0222	0.0134	-0.0149
34.74	3.54	2.51	2.34	-0.51	-0.0047	0.0011	-0.0005	-0.0004	-0.0012	0.0207	0.0113	0.0046
40.60	4.41	2.61	4.12	-1.70	-0.0171	-0.0284	-0.0333	-0.0284	0.0170	0.0291	0.0408	0.0125
50.36	4.81	2.48	4.18	-1.57	0.0092	-0.0028	0.0326	-0.0322	0.0682	-0.0337	0.0328	-0.0140
55.01	4.75	2.52	1.47	-0.96	0.0006	0.0258	0.0049	-0.0006	0.0706	-0.0313	-0.0088	0.0053
60.51	4.47	2.58	6.30	-4.07	-0.0249	-0.0212	-0.0232	0.0033	0.0414	-0.0283	-0.0299	-0.0229
64.35	4.26	2.59	6.39	-5.22	-0.0188	-0.0128	0.0012	0.0034	0.0343	-0.0647	-0.0512	-0.0373
75.31	4.61	2.59	1.50	-8.43	0.0559	0.0165	0.0051	0.0296	-0.0757	0.1029	-0.0844	-0.0409
81.95	4.42	2.68	0.82	-5.59	0.0106	-0.0077	-0.0420	0.0137	-0.0760	0.0302	-0.0496	-0.0956
94.99	4.87	2.61	16.01	-11.23	-0.0075	-0.0325	-0.0025	-0.0046	-0.0066	-0.0719	-0.1254	-0.0435
105.29	4.62	2.62	18.72	-12.07	-0.0060	-0.0412	0.0005	0.0067	-0.0395	-0.0511	-0.0875	-0.0468
117.14	3.98	2.56	15.04	-8.77	-0.0126	0.0157	0.0046	0.0436	-0.0390	-0.0909	-0.0320	-0.0147
128.96	3.50	2.61	17.81	-8.89	-0.0006	-0.0119	0.0028	0.0689	-0.0274	-0.0943	-0.0247	-0.0225
136.46	4.02	2.65	20.19	-10.51	0.0259	-0.0087	-0.0047	0.0312	0.0076	-0.0871	-0.0048	-0.0292
147.32	3.90	2.61	14.48	-15.27	0.0028	0.0074	0.0185	0.0288	-0.0085	-0.0677	0.0053	-0.0343
164.56	4.49	2.66	8.04	-13.69	-0.0134	-0.0385	-0.0024	0.0068	0.0442	0.0291	0.0383	-0.0433

F04

TABLE 4 - GALAXY 2 (NGC 6173)

R	ε	θ	x_0	y_0	A_1	B_1	A_2	B_2	A_3	B_3	A_4	B_4
10.31	3.25	0.73	0.0	0.0	0.0003	-0.0005	-0.0013	0.0005	0.0053	-0.0029	-0.0019	-0.0058
11.21	3.24	0.72	-0.15	-0.08	0.0	0.0001	-0.0018	-0.0003	-0.0010	-0.0104	-0.0033	-0.0001
12.29	3.34	0.72	0.05	-0.08	0.0026	0.0002	-0.0007	0.0004	-0.0012	0.0007	0.0053	0.0066
13.61	3.33	0.70	-0.11	-0.03	-0.0005	0.0003	0.0013	-0.0005	-0.0052	-0.0035	0.0002	0.0002
14.51	3.37	0.71	-0.08	0.01	0.0001	-0.0002	0.0001	0.0019	0.0009	-0.0007	0.0001	0.0022
15.64	3.47	0.72	-0.14	-0.02	0.0010	-0.0013	-0.0009	0.0007	0.0027	-0.0059	-0.0051	0.0053
17.19	3.58	0.71	-0.31	-0.08	-0.0019	0.0025	-0.0020	-0.0018	-0.0040	-0.0017	-0.0050	0.0071
19.05	3.73	0.70	-0.70	-0.14	0.0012	-0.0018	-0.0007	0.0028	-0.0087	-0.0045	-0.0061	-0.0051
20.06	3.79	0.70	-0.48	-0.08	-0.0017	0.0009	-0.0019	-0.0013	0.0004	0.0009	-0.0052	-0.0079
21.21	3.80	0.72	-0.35	-0.08	0.0016	-0.0052	-0.0036	0.0014	-0.0054	0.0074	-0.0010	-0.0040
22.36	3.74	0.70	-0.42	-0.15	-0.0047	0.0084	-0.0004	0.0008	0.0001	0.0156	-0.0017	-0.0059
23.86	3.75	0.72	-0.30	-0.19	0.0022	-0.0008	-0.0031	0.0013	0.0012	0.0080	0.0020	-0.0164
25.65	3.60	0.70	-0.40	-0.22	0.0064	-0.0030	0.0033	0.0065	0.0050	-0.0007	-0.0003	-0.0130
27.79	3.59	0.70	-0.65	-0.33	0.0037	0.0017	0.0051	-0.0002	0.0162	0.0080	0.0081	-0.0156
30.34	3.65	0.68	-0.13	0.02	0.0007	0.0024	0.0024	0.0009	0.0020	0.0181	-0.0095	-0.0176
32.84	3.25	0.67	0.00	-1.18	-0.0165	-0.0057	-0.0023	0.0143	-0.0127	0.0053	-0.0225	-0.0101
36.91	3.37	0.63	-0.23	-0.78	0.0028	-0.0038	0.0060	0.0059	0.0022	-0.0051	-0.0066	-0.0113
43.05	3.41	0.58	-2.65	-2.14	-0.0112	-0.0059	-0.0010	-0.0021	0.0176	-0.0342	-0.0044	-0.0049
44.92	3.66	0.61	-3.59	-2.21	0.0005	-0.0063	-0.0011	-0.0098	0.0405	-0.0148	0.0183	-0.0133
46.63	3.61	0.61	-2.73	-2.17	0.0056	0.0038	-0.0034	-0.0006	0.0295	-0.0134	0.0176	-0.0114
49.80	4.22	0.65	-6.59	-2.27	0.0011	0.0006	-0.0053	-0.0043	0.0484	0.0328	0.0305	0.0190
53.33	4.38	0.61	-5.57	-2.68	0.0093	0.0005	-0.0114	0.0006	0.0367	0.0030	0.0157	0.0108
57.43	4.54	0.57	-5.28	-2.69	-0.0043	-0.0061	-0.0028	-0.0059	-0.0374	0.0348	0.0196	-0.0004
63.73	4.82	0.54	-7.47	-4.10	0.0071	0.0137	-0.0140	0.0027	-0.0205	-0.0309	0.0061	-0.0007
70.14	4.89	0.50	-9.35	-2.61	-0.0034	-0.0059	0.0174	-0.0030	-0.0170	0.0144	0.0162	-0.0073
78.41	4.65	0.46	-13.61	-4.78	-0.0136	0.0039	0.0098	0.0054	-0.0378	0.0251	-0.0091	-0.0006
92.69	2.88	0.40	-22.83	-1.81	-0.0154	-0.0101	0.0169	0.0540	-0.0507	0.0282	0.0465	-0.0071
115.08	3.94	0.57	-13.36	0.36	-0.0212	-0.0346	-0.0247	-0.0030	0.0674	0.0581	0.0490	0.0426
123.50	3.79	0.42	-8.32	7.51	0.0021	-0.0514	0.0287	-0.0217	0.0718	-0.0127	0.0793	-0.0385
132.39	3.41	0.55	-8.91	4.84	-0.0061	-0.0065	-0.0123	0.0219	0.0367	0.0307	0.0532	-0.0111
142.56	4.57	0.51	10.79	8.51	0.0050	-0.0603	0.0074	-0.0578	0.0258	0.0342	0.0301	0.0013

F05

TABLE 5 - GALAXY 5 (NGC 6159)

R	ε	θ	x_0	y_0	A_1	B_1	A_2	B_2	A_3	B_3	A_4	B_4
10.44	2.66	2.34	0.0	0.0	-0.0087	0.0101	-0.0046	0.0018	-0.0149	-0.0021	0.0014	-0.0036
11.47	2.64	2.31	-0.05	-0.16	0.0060	0.0051	-0.0092	0.0049	-0.0001	-0.0024	0.0003	-0.0206
12.93	2.67	2.29	-0.06	-0.15	-0.0009	0.0015	-0.0037	0.0060	0.0017	0.0062	-0.0038	-0.0055
13.58	2.82	2.31	-0.11	-0.19	0.0005	0.0041	-0.0086	-0.0037	-0.0002	0.0093	0.0026	-0.0187
14.33	2.79	2.30	-0.07	-0.37	0.0080	0.0088	-0.0033	-0.0045	0.0036	0.0112	0.0106	-0.0192
15.23	2.73	2.28	-0.02	-0.34	0.0066	-0.0023	-0.0020	0.0005	0.0068	0.0053	0.0046	-0.0152
16.38	2.56	2.24	0.02	-0.08	-0.0060	0.0017	0.0036	0.0015	-0.0005	0.0026	-0.0187	-0.0041
17.74	2.73	2.26	-0.20	-0.21	-0.0009	-0.0156	-0.0021	-0.0079	-0.0043	-0.0122	-0.0087	-0.0173
19.47	2.62	2.28	0.08	-0.09	-0.0038	0.0080	0.0003	-0.0019	0.0111	0.0021	-0.0001	-0.0229
21.87	2.58	2.25	0.24	-0.47	0.0034	0.0026	-0.0037	0.0101	-0.0051	0.0059	-0.0084	-0.0048
24.90	2.55	2.22	0.07	0.06	-0.0011	-0.0032	0.0019	0.0070	-0.0089	0.0148	-0.0165	-0.0089
30.44	2.49	2.20	0.83	0.25	-0.0231	0.0050	0.0048	0.0106	0.0022	0.0182	-0.0188	-0.0091
46.28	2.90	2.20	0.67	-0.26	0.0023	-0.0129	0.0142	0.0010	0.0303	-0.0004	0.0084	-0.0220
54.10	2.63	2.34	1.94	-0.55	-0.0129	0.0091	0.0016	-0.0183	-0.0158	0.0228	-0.0072	-0.0389
64.81	4.15	2.14	8.27	2.29	0.0330	0.0180	0.0335	-0.0274	-0.0086	0.0867	-0.0378	0.0603
69.54	4.27	2.10	13.02	2.21	0.0291	-0.0279	0.0438	-0.0044	0.0055	0.1083	-0.0137	0.0765

F07 F08

TABLE 6 - GALAXY 11

R	ε	θ	x_0	y_0	A_1	B_1	A_2	B_2	A_3	B_3	A_4	B_4
9.87	3.10	0.51	0.0	0.0	0.0069	-0.0029	0.0035	-0.0124	-0.0181	-0.0063	0.0035	0.0007
11.47	2.51	0.56	-0.10	-0.06	-0.0120	-0.0206	0.0103	0.0137	0.0051	0.0164	0.0051	-0.0030
12.35	2.77	0.64	-0.14	0.01	0.0034	0.0024	-0.0039	0.0	-0.0026	0.0035	-0.0205	-0.0178
12.84	2.87	0.65	-0.35	0.05	-0.0013	-0.0015	-0.0039	-0.0002	0.0046	0.0011	-0.0215	-0.0125
13.33	2.91	0.66	-0.49	0.15	-0.0037	-0.0037	-0.0046	0.0003	0.0076	0.0002	-0.0221	-0.0094
14.00	3.21	0.67	-0.06	0.11	0.0001	-0.0025	-0.0036	0.0010	-0.0092	0.0224	-0.0206	0.0067
14.71	3.00	0.70	0.02	0.11	-0.0084	-0.0029	-0.0083	0.0104	-0.0113	0.0270	-0.0173	0.0046
15.59	2.38	0.72	-0.02	0.64	0.0055	0.0	-0.0047	0.0288	0.0078	0.0275	-0.0066	0.0223
16.62	2.16	0.70	0.19	0.81	0.0056	0.0008	0.0001	0.0228	0.0280	0.0123	0.0082	0.0116
18.02	2.40	0.82	0.47	0.34	-0.0027	-0.0053	-0.0180	0.0115	0.0425	-0.0054	0.0234	0.0276
19.79	1.95	0.95	0.78	-0.68	-0.0148	-0.0035	-0.0215	0.0294	0.0755	-0.0149	0.0201	0.0192
23.78	2.11	0.62	3.78	-0.96	-0.0229	-0.0565	-0.0392	-0.0095	-0.0118	-0.0614	-0.0662	-0.0067
24.60	1.49	0.66	3.65	-0.99	-0.0213	-0.0374	-0.0345	0.0174	-0.0071	-0.0780	-0.0596	-0.0079
26.38	1.60	1.32	1.46	2.89	-0.0296	-0.1301	-0.0503	-0.0849	-0.0344	-0.0848	0.0490	-0.0236
29.66	1.97	1.01	2.56	1.91	0.0286	0.0274	-0.0261	0.0215	0.0709	0.0202	-0.0345	-0.0046
31.94	1.99	1.06	2.49	2.43	0.0094	0.0077	0.0072	0.0102	0.0515	0.0738	-0.0458	-0.0353

F09 F10